UNIVERSITY OF TWENTE.

Faculty of Electrical Engineering, Mathematics & Computer Science

Light detection at low temperatures in silicon photodiodes

Céline Steenge

B.Sc. Thesis
June 2018

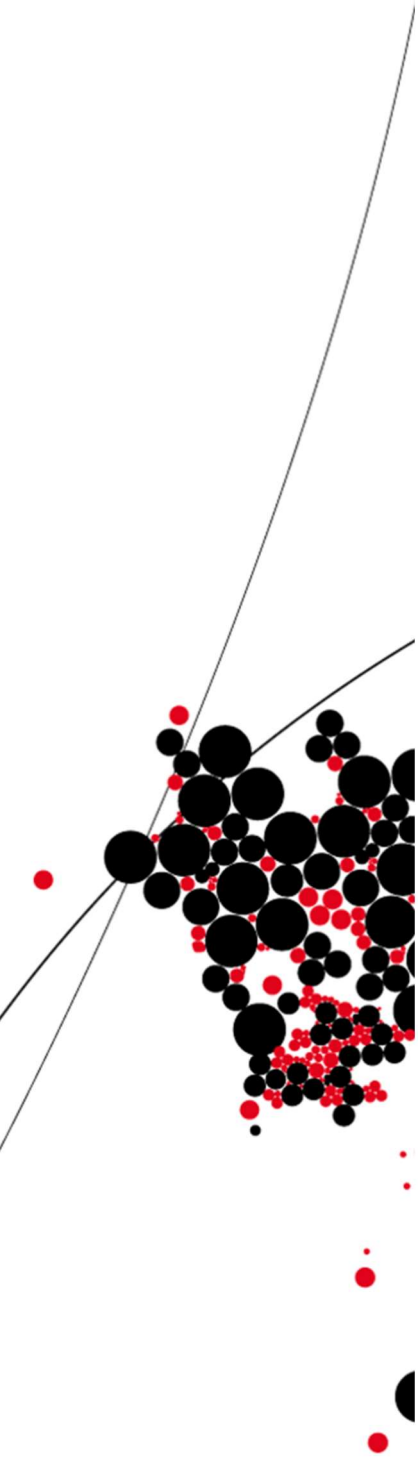

Supervisors:
Dr.ir. Ray Hueting
Dr.ir. Anne-Johan Annema

Integrated Devices and Systems Group
Faculty of Electrical Engineering,
Mathematics and Computer Science
University of Twente
P.O. Box 217
7500 AE Enschede
The Netherlands

Summary

Applications such as aerospace have a strong desire for good functional electric circuits which could work at ultralow (cryogenic) temperatures. A potential device could be the silicon (avalanche) photodiode. However, almost no research has been performed on the influence of light on photodiodes at cryogenic temperatures. The knowledge gained during this research will also be used on Bipolar Junction Transistors (BJT) and Metal-Oxide-Semiconductors at cryogenic temperatures and with light influence.

This research will have the main research question:*'what is the influence of temperature on light detection in silicon photodiodes?'*. From this main research question, it can be discussed whether or not the conventional photodiode is more appropriate for light detection at low temperatures than the avalanche photodiode (APD). In order to answer this question, two sub research questions have been formulated: *'what is the influence of the temperature on the breakdown voltage of silicon photodiodes?'* and *'what is the influence of light on the breakdown voltage of silicon photodiodes at cryogenic temperatures?'*. The approach was to analyse the diodes both electrically and opto-electrically for a wide temperature range.

The conventional photodiode is a semiconductor device that can convert light into electrical current. The photon energy should be equal or larger than the band gap energy of, in this case, silicon. The absorption coefficient should be such that the generation and recombination takes place in the depletion layer. The avalanche photodiode is biased near the break down voltage and will cause an avalanche of electron-hole pairs, resulting in a large negative current. The Zener diode is designed to have a current flow in both the forward and reverse direction. The Zener diode is highly doped and therefore has a high electric field. The Zener effect and the avalanche breakdown contribute in the breakdown region under different ratios.

All the diodes have multiple relations to temperature and light. The Shockley diode equation, the thermal voltage, the band gap energy and the breakdown voltage are temperature dependent. The photon energy, the Shockley diode equation, the responsivity and the quantum efficiency are light dependent.

On the chip, diode type 2.1 was chosen for this research. The photodiode was bonded on the sample holder and measured electrically with the Keithley 4200-SCS and the ProbeShield M300 waferprober with controlled heater/cooler. The diode was measured opto-electrically with the Keithley 4200-SCS and the Oxford Instruments cryostat.

The probestation gave a breakdown voltage around -4.5 V. The cryostat gave a breakdown voltage around -3 V. In both cases, it was noticeable that the diodes did barely react to light.

The results show noise between -2 V and 0 V for the probestation and between -3 V and +0.7 V

for the cryostat. Furthermore, a negative temperature coefficient is visible in both the probestation and cryostat measurements. Next, almost no reaction to light can be found in the various figures. The breakdown for the probestation is between -4.0 V and -5.0 V. The breakdown for the cryostat is between -4.0 V and -3.0 V.

Since the temperature coefficient is negative, the diode does not react to light and the diode is highly doped, it is likely that diode is a Zener diode. However, also a vertical diode could influence the measurements. This vertical diode is also insensitive to light and could have a negative temperature coefficient.

Additionally, it was recognized that the 5K and 23K and the 433K and 473K curve were swapped. This could be due to more avalanche breakdown than Zener effect at cryogenic temperatures for the 5K and 23K and the opposite for the 433K and 473K. Moreover, tunneling is less likely at lower temperatures and more likely at higher temperatures.

Trap assisted tunneling (TAT) could also influence this diode. The Shockley-Read-Hall (SRH) recombination could be stimulated. However, SRH recombination, Zener effect and TAT become less dominant at lower temperatures, meaning that avalanche will take over.

The noise mentioned earlier is most likely leakage currents due to the design of the diode, but Zener diodes are also known for their high noise. The vertical diode could also produce noise in the measurements which change with temperature. The noise of the probestation was measured in various cases and was 10 pA. Bonding could also play a role in the noise.

To conclude, the research questions get a different meaning when using a Zener diode. The negative temperature coefficient of the Zener diode showed to be true, but the avalanche breakdown seems to dominate at extreme low temperatures. The relatively small depletion region made that there was limited to no light absorption, so no conclusion could be found. Since the second sub question could not be answered, given this Zener diode, the main research question can also not be answered.

Further research is needed in the field of temperature relations for the (Zener) diode; photodiodes at cryogenic temperatures and light reaction; diode design for this specific research; responsivity of Si photodiodes at cryogenic temperatures and the detection of near infrared in Zener diodes.

The most important recommendation is the change of diode design. During the research, multiple obstacles were found due to the design of the diode. When the design would change, better research could be performed based on the previous stated research questions.

Next, the measurement set-up should be changed to a set up which is both applicable to electrically and opto-electrically measurements.

Acknowledgement

I would like to thank Dr.ir. R.J.E. Hueting and Dr.ir. A.J. Annema for guiding me through the research and giving me the chance to help them out with this subject. Furthermore I would like to thank ing. H. de Vries, ing. J.G.M Sanderink and ing. J.P. korterik for helping with the measurement set ups. Moreover I want to thank Dimitri Geskus from Lionix for bonding our chips to the sample holders. Next, I want to thank Prof.dr. J. Schmitz for joining my Bachelor Assignment Committee. Lastly, I want to thank everyone I asked for reading my Bachelor thesis.

Contents

Summary ii

Acknowledgement iv

1 Introduction 1
1.1 Motivation . . . 1
1.2 Research questions and approach . . . 1
1.3 Report organization . . . 2

2 Theory 3
2.1 Photodiodes . . . 3
2.2 Relations . . . 5

3 Method 10
3.1 Samples . . . 10
3.2 Measurements . . . 13

4 Results 15
4.1 Electrical measurements . . . 15
4.2 Electro-optical measurements . . . 21

5 Discussion 25

6 Conclusions and recommendations 29
6.1 Conclusions . . . 29
6.2 Recommendations . . . 29

List of abbreviations and symbols 31

References 1

Appendices

A Chip data 3
A.1 Diode types . . . 3
A.1.1 Diode type 1 . . . 3
A.1.2 Diode type 2 . . . 7
A.1.3 Diode type 3 . . . 11

B Measurement equipment **17**
B.1 Keithley 4200 semiconductor characterization system 17
B.2 Photo's measurement devices 18

C Optical measurements **23**
C.1 Theoretical set-up 23
C.2 Calculations 24
C.3 Actual set-up 25

Chapter 1

Introduction

This introduction describes the motivation, the research questions and the report organization of the bachelor assigned performed in the Integrated Devices and Systems (IDS) group and the Integrated Circuit Design (ICD) group of the University of Twente (UT).

1.1 Motivation

For applications such as aerospace, quantum computing or counting pulses with low noise and low power consumption, there is a strong desire for good functional electric circuits which could be used at ultralow (e.g. cryogenic) temperatures. One potential device for this is the silicon (avalanche) photodiode. Such a diode could be used, for instance, as a key component current source circuit in such systems. In order to see whether this is possible, research is needed. Although research has been done on photodiodes at lower temperatures (till 100K) or light detection, almost no research has been done at cryogenic temperatures with the influence of light. After this research, the knowledge gained will also be used for more research on Bipolar Junction Transistors and Metal-Oxide-Semiconductor at cryogenic temperatures and with light influences. This research will mostly focus on the reverse biased photodiodes used for light detection.

This research is useful for the groups and the University of Twente. Therefore, both research groups contributed to this research.

1.2 Research questions and approach

This research is based on the main research question:

- What is the influence of temperature on light detection in silicon photodiodes?

From this main research question, it can be discussed whether or not the conventional photodiode is more appropriate for light detection at low temperatures than the avalanche photodiode (APD). In order to answer this question, two sub research questions have been formulated:

1. What is the influence of the temperature on the breakdown voltage of silicon photodiodes?
2. What is the influence of light on the breakdown voltage of silicon photodiodes at cryogenic temperatures?

During the report, these questions will be answered and conclusions will be drawn.

The approach is to analyse diode samples both electrically and opto-electrically for a wide temperature range. These samples were realised in a 65 nm bulk CMOS process provided by the company TSMC (Taiwanese Semiconductor Manufacturing Company). More information about the chip can be found in appendix A.

1.3 Report organization

The report is organized as follows. In chapter 2, the theoretical background of the photodiode and APD is explained. Then, in chapter 3, the measurement method and the sample details are described. Chapter 4 shows the measurements and chapter 5 discusses these results. Finally, in chapter 6, conclusions are drawn and recommendations are given. All abbreviations and symbols found in the report can be mentioned in the list of abbreviations and symbols.

Chapter 2

Theory

This chapter contains some basic theory on the conventional photodiode and the avalanche photodiode. Based on the theory, the temperature and light relations for the current-voltage (I-V) curves of the photodiodes are stated which are needed for the research.

2.1 Photodiodes

A photodiode is a semiconductor device that can convert light into electrical current. In the semiconductor, the generation of electron-hole pairs takes place when an electron has gained sufficient energy to jump from the valence band to the conduction band. Moreover, during the generation and recombination process, lattice vibrations (phonons) are produced. The energy for this should be equal to or larger than the band-gap energy [eV] (E_g) of, in this case, silicon (Si). The light that shines on the Si provides the electron with the energy of quantum light. This absorption principle will therefore mainly work when the energy of quantum light is equal or larger than E_g [1].

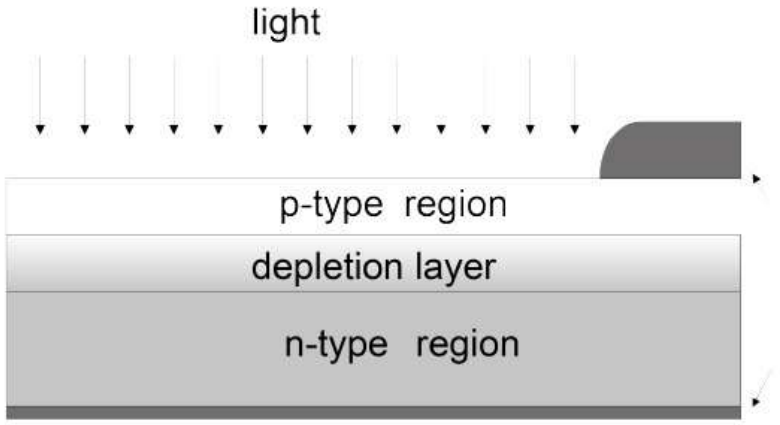

Figure 2.1: schematic cross-section of the photodiode. [2]

Figure 2.1 shows a schematic cross-section of the photodiode. When the absorption coefficient in the Si is very large, the electron-hole pairs will be mainly generated in the p-type neutral region. When the absorption coefficient is very small, the electron-hole pairs will be generated in the n-type neutral region. It is preferred to have the generation process in the depletion layer [2]. The absorption

coefficient in Si at room temperature can be approximated with [3]:

$$\alpha \approx 10^{13.2131-36.7985\lambda+48.1893\lambda^2-22.5562\lambda^3}, \tag{2.1}$$

with absorption coefficient $[\frac{1}{\mathrm{cm}}]$ (α) and wavelenght of light [μm] (λ).

The α can, for example, be tuned by adopting another semiconductor [1]. When an electron-hole pair is generated in the depletion layer, the electric field will separate the carriers. Due to this, a photocurrent is formed, which is a relatively fast and efficient process. When the electron-hole pairs are in the neutral regions, especially those with a diffusion length away from the depletion layer, the electrons and holes will most likely recombine, meaning that they will not contribute to the photocurrent. When the pairs do however reach the depletion layer, they still contribute via diffusion, which is relatively slow process [2].

According to equation 2.1 and the text above, Si photodiodes are only sensitive for a particular wavelength range. Above a wavelength of 950 nm, the photon energy does not reach the band gap energy. Below 400 nm wavelength, the excess carries are generated in the upper region and not the depletion region of the photodiode and will likely not contribute to the photocurrent. The typical spectral range of Si photodiodes will be from 400 to 950 nm [3].

Avalanche photodiodes

As the process explained for the conventional photodiode, the APD has almost the same principle. However, the APD is biased near the break-down voltage hence in avalanche mode. Due to the high electric field in the semiconductor, the carriers will speed up and move. This causes a collision with the crystal lattice, which creates more electron-hole pairs. Some of these newly created carriers then undergo the same process, resulting in a quick increase of electron-hole pairs and consequently a large negative current [4]. The difference with the conventional photodiode is therefore also the gain in current. The gain of the APD is larger than the gain of the conventional photodiode. However, unlike in a conventional photodiode more direct energy transitions are possible, hence less phonons are required, because of the high field [5].

After the avalanche, the APD should have a lower reverse voltage in order to return to its normal state. This can easily be done by placing a series resistor in the voltage supply line which causes quenching. For more information about this, see avalanche photodiodes and quenching circuits [6].

Zener or tunnel diode

The Zener or tunnel diode [7], [8] has a different working principle than the avalanche photodiode, but also makes use of the avalanche breakdown. The diode is designed to have current flow in both the forward and reverse direction. The p-n junction is highly doped and consequently the diode has a high electric field [9], [10]. The Zener diode makes use of the Zener effect (electron quantum tunneling), as is visible in figure 2.2, but also of the avalanche breakdown [9], [10].

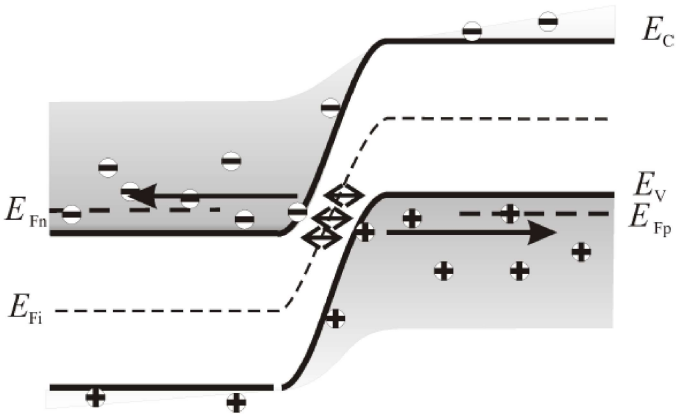

Figure 2.2: Zener effect in Zener diode (reversely biased). [11]

For the Zener diode it is known that the breakdown mechanism below approximately 5 V for Si is band-to-band tunneling with a negative temperature coefficient [1]. Between 5 and 7 Volt for Si, the breakdown mechanism is a combination of band-to-band tunneling and avalanche multiplication and for 7V or higher, the breakdown mechanism is mainly avalanche multiplication [1]. However, in practice because of the heavily doped implementations, traps in or near the junction could be formed. This could result in trap-assisted tunneling [12], causing a more temperature dependent tunneling. Typically, Zener diodes exhibit of relatively large electronic noise [13].

2.2 Relations

Since temperature and light play a big role in the research, it is important to know which characteristics are influenced by the temperature and light.

Temperature

The first logical relation to keep in mind focusing on the temperature is the diffusion current of a short diode:

$$I = I_{\mathrm{o}} \left(\exp\left(\frac{V_{\mathrm{D}}}{\mathrm{n} \cdot U_T} \right) - 1 \right) = qAn_{\mathrm{i}}^2 \left\{ \frac{1}{N_{\mathrm{A}}} \frac{D_n}{L_p} + \frac{1}{N_{\mathrm{D}}} \frac{D_p}{L_n} \right\} \left(\exp\left(\frac{V_{\mathrm{D}}}{\mathrm{n} \cdot U_T} \right) - 1 \right) \tag{2.2}$$

$$U_T = \frac{k \cdot T}{q}, \tag{2.3}$$

with reverse saturation current [A] (I_o), voltage across the diode [V] (V_D), ideality factor (n), elementary charge (q), active photodiode area [cm^2] (A), intrinsic carrier concentration [cm^{-3}] (n_i), doping concentration acceptor [cm^{-3}] (N_A), diffusion coefficient electron [$\frac{\mathrm{cm}^2}{\mathrm{s}}$] ($D_n$), length of n layer [cm] (L_n), doping concentration donator [cm^{-3}] (N_D), diffusion coefficient hole [$\frac{\mathrm{cm}^2}{\mathrm{s}}$] ($D_p$), length of p layer [cm] (L_p), Boltzmann constant (k) and temperature [K] (T).

In equation 2.2 (the Shockley diode equation [11]), one can see the dependence of temperature in the thermal voltage U_T. The thermal voltage is shown in equation 2.3. It is however important to know that when the photodiode is reversely biased, in ideal situations the exponential term vanishes.The reverse bias saturation current will remain, which has the temperature dependent n_i [2]:

$$n_i = \sqrt{N_{\mathrm{c}} N_{\mathrm{v}}} \cdot \exp\left(-\frac{E_{\mathrm{g}}}{2kT} \right), \tag{2.4}$$

with conduction band effective density-of-states [cm^{-3}] (N_C) and valence band effective density-of-states [cm^{-3}] (N_V).

In less ideal situations, the reverse current is either limited by the thermal generation or by tunneling (Zener effect) [1].

As a second order effect, the band gap energy is influenced by the temperature. As

$$E_{\mathrm{g}}(T) = E_{\mathrm{g}}(0) - \frac{\alpha T^2}{T+\beta}, \tag{2.5}$$

with the band gap energy at 0 Kelvin ($E_g(0)$) and silicon specific constants (α and β). [14], the band gap energy for T bigger than 0 Kelvin is smaller than the band gap energy at 0 Kelvin. This means that less energy is needed to jump over the band gap at higher temperatures. "*With decreasing temperature a contractions of the crystal lattice this usually leads to a strengthening of the interatomic bonds and an associated increase in the band gap energy.*" [14]. However, for silicon the band gap energy varies from 1.170 eV to approximately 1 eV for a temperature range of 0 to 600 K [15] (see figure 2.3). This means that this difference might not be significant.

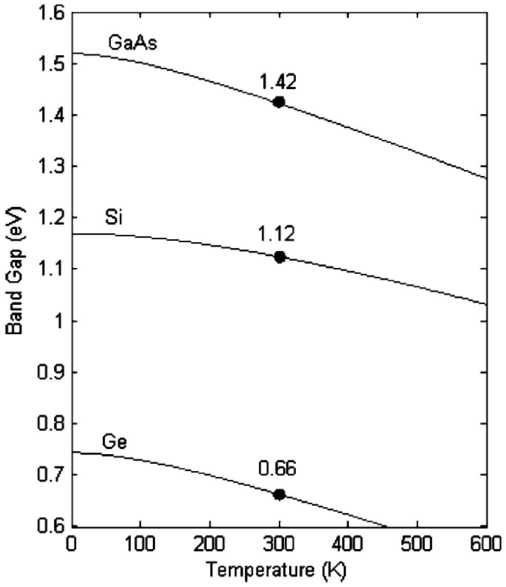

Figure 2.3: band gap - temperature graph showing the effect of temperature on the band gap energy for GaAs, Si and Ge. [15]

Moreover, Si has several high energy interbands which are shown in figure 2.4. Here it is visible that the band gap at 1.1 eV to the conduction band is not directly above the valance band, and therefore phonons are needed as well during practically any transition. When no phonons are available (which is most likely the case at low temperatures), the indirect band gaps needs to be bridged. By applying a high reverse bias, hence energy, there are more electrons higher in the conduction band. As a result more direct transitions are within reach. This band gap has a higher band gap energy and can therefore absorb visible light as well [5].

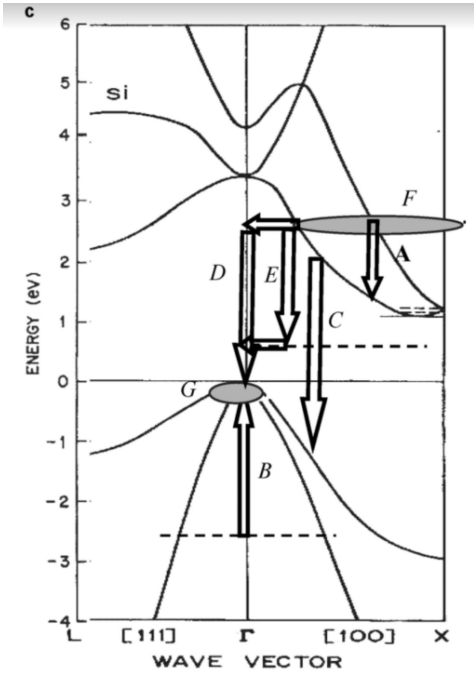

Figure 2.4: *"possible photonic energy transitions for the device in the Si band diagram."* [5]

Lastly, the break-down voltage depends on temperature. Focusing on avalanche breakdown, at room temperature, the electrons will scatter with the Si lattice, causing the avalanche at elevated temperatures.

The carriers lose more energy to the crystal lattice along a given distance with a constant field because of increased lattice vibrations (phonons). This results in a lower ionization rate. Therefore, the carries must pass through a higher voltage before the photons have enough energy to generate electron-hole pairs [1].

Since this lattice is vibrating, the electrons will be slowed down. When the lattice is static, the electron scatter with full speed [1]. This means that at low temperatures, the electrons have more speed at the same voltage compared to room temperature. Therefore, the avalanche breakdown voltage will decrease. Vice versa, when the temperature increases, the break-down voltage increases as well [1], [16].

Furthermore, there is also a second order effect that the break-down voltage is related to the dark current. In the photoconductive mode, the dark current approximately doubles for every 10 degrees Celsius increase change in temperature [17]. This also implies that when the temperature is low, the dark current will come close to zero, here the breakdown voltage reduces further.

Low temperatures (below 100K), the doping will not all be activated, meaning that effectively N_D will be lower. Due to this, the slope of the electric field will be less steep. This is visible in:

$$\frac{\partial \varepsilon}{\partial x} = \frac{\rho}{\epsilon_s} \approx \frac{qN_D}{\epsilon_s}, \tag{2.6}$$

$$\varepsilon = \int_0^W \frac{qN_D}{\epsilon_s} dx = -\frac{qN_D\,(W-x)}{\epsilon_s}, \tag{2.7}$$

with electric field [$\frac{\mathrm{V}}{\mathrm{cm}}$] ($\varepsilon$), charge density [$\frac{\mathrm{C}}{\mathrm{cm}^3}$] ($\rho$), permittivity [$\frac{\mathrm{F}}{\mathrm{cm}}$] ($\epsilon_s$) and width of the n layer (W) [1]. Knowing that the breakdown field causes avalanche breakdown and that the integral of the electric field at the breakdown field is the breakdown voltage [1], figure 2.5 shows that the breakdown voltage will increase for lower N_D. Therefore, the breakdown voltage will increase at lower temperatures.

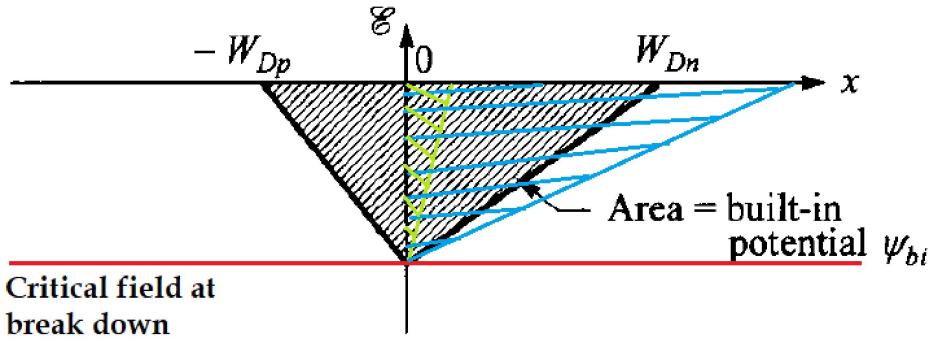

Figure 2.5: the electric field distribution for three doping levels. [1]

Finally, one thing to keep in mind is that the Zener diode has a negative temperature coefficient for the breakdown voltage. This is due to the Zener effect below 5 V and the combination of Zener effect and avalanche breakdown between 5 V and 7 V. The avalanche breakdown has a positive temperature coefficient (see [1], [9], [10]). Also, the Zener effect could become less important once the doping is less activated. To complicate things further, trap-assisted tunneling on the other hand has a positive temperature dependence.

So, to extensively investigate the temperature dependence many physical effects could play a role and therefore a carefully designed set of experiments is required.

Light

Zener diodes have a relatively small depletion width compared to the conventional or avalanche photodiode. This means that the region where light could be captured is relatively small. Therefore, light absorption is hardly seen in the I-V curve of a Zener diode. For conventional and avalanche photodiodes on the other hand, the following is true.

Light creates electron-hole pairs, but photons will also affect other characteristics. For the photon energy holds [1]:

$$E_{\text{photon}}(eV) = h \cdot v = \frac{hc}{\lambda(\mu m)} = \frac{1.2398}{\lambda(\mu m)}, \tag{2.8}$$

with Planck's constant (h), speed of light (c) and frequency of photon [Hz] (v).

Hence the photon energy depends on the wavelength: photons with shorter wavelengths have more energy than those with longer wavelengths. This photon energy needs to be higher than the band-gap energy to make an electron jump across the band-gap.

Moreover, the photocurrent equation [2] can be found in:

$$I_{\text{L}} = \frac{\eta \cdot q \cdot A \cdot I_{\text{illum.}}}{h \cdot v} = \frac{\eta \cdot q \cdot A \cdot I_{\text{illum.}} \cdot \lambda}{h \cdot c}, \tag{2.9}$$

with quantum efficiency (η) and intensity of illumination [$\frac{\text{W}}{\text{cm}^2}$] ($I_{illum.}$). The photocurrent is affected by the wavelength.

The light illumination changes the Shockley equation (2.2) to [2]:

$$I_D = I_0 \left(\exp\left(\frac{V_{\text{AC}}}{n \cdot U_T} \right) - 1 \right) - I_{\text{L}} \tag{2.10}$$

From equation 2.10, the effect in figure 2.6 can be explained. The variables for the photocurrent are the intensity of illumination and the photon wavelength. When the illumination intensity becomes larger with a constant photon wavelength, the total current becomes more negative. This results is visible in figure 2.6 by the curves P_0, P_1 and P_2 (in increasing order). Each curve represents an I-V curve with a different light intensity.

When the photon frequency becomes smaller with a constant light intensity, the total current also becomes more negative. This will be until the photon frequency will not reach the depletion region anymore. From then on, no effect of light will be visible. The same effect as with the change in light intensity will occur.

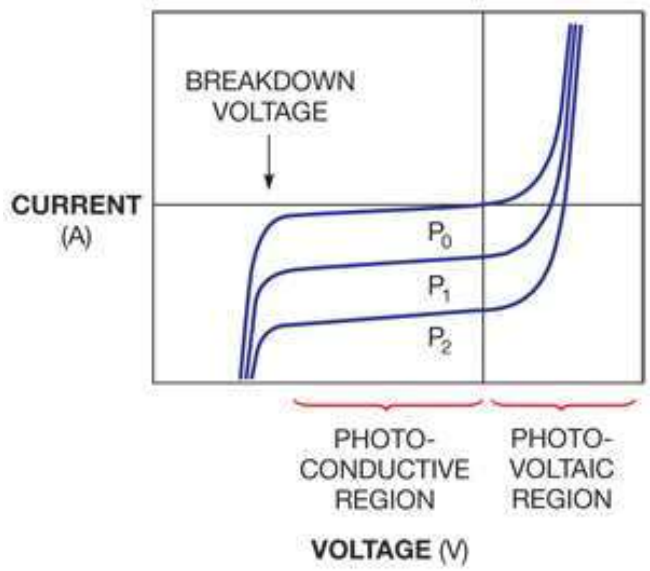

Figure 2.6: I-V curve of a photodiode. P_0, P_1 and P_2 (increasing order) show the influence of different light levels [18].

Thirdly, the responsivity [$\frac{\mathrm{A}}{\mathrm{W}}$] ($R_{lambda}$) of Si photodiodes is a measure of sensitivity of light [1], [19]. Equation 2.11 shows that the responsivity also depends on the light ratio of of the photocurrent I_P.

$$R_{\mathrm{lambda}} = \frac{I_P}{P_{\mathrm{optical}}} = \frac{\eta q}{hv} = \frac{\eta \lambda\,(\mu\mathrm{m})}{1.2398}, \tag{2.11}$$

with input power [W] (P). The responsivity shows how effective the conversion of light power into electrical current is. This relation is also visible in figure 2.6, where the distance between the lines in the photoconductive region is equal to I_P. Changes in temperature also have an effect on the responsivity due to the changing band gap.

Lastly, the quantum efficiency η [1], [19],

$$\eta = R_{\mathrm{lambda}} \cdot \frac{h \cdot c}{\lambda \cdot q} = R_{\mathrm{lambda}} \cdot \frac{h \cdot v}{q}, \tag{2.12}$$

which is the number of electron-hole pairs generated per incoming photon. This also shows a relation with the responsivity and the wavelength λ. This is due to the fact that the photons that hit the photodiode need to have the correct energy and should influence as much as possible carriers.

Chapter 3

Method

This section describes how the experiments were performed and with which equipment. The chosen photodiode sample is discussed together with the measurement equipment. The measurement devices can be found in appendix B.

3.1 Samples

Since the chip with the photodiodes is used for multiple researches, multiple designs can be found on the chip. The chosen photodiode (designed by ICD in a 65 nm bulk CMOS process provided by TSMC) for this research is diode type 2.1, which can be found in figure 3.1, 3.2, 3.3 and 3.4. It is important to know that the photodiode is highly doped. For more data on the photodiode and the other photodiodes, see appendix A.

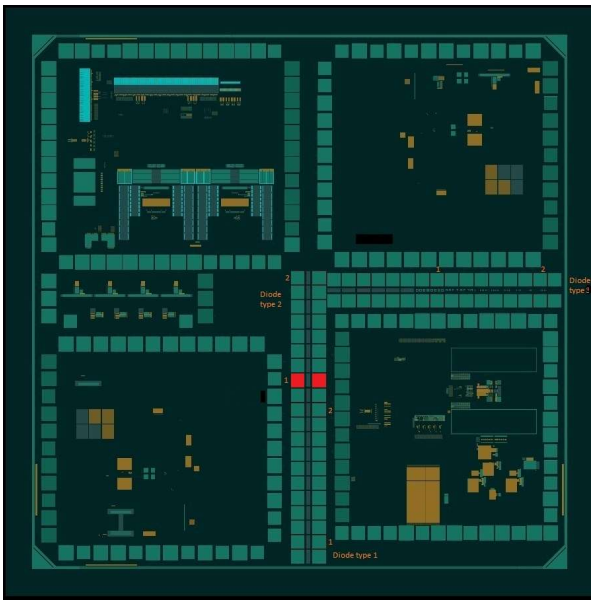

Figure 3.1: Layout (topview) of the full chip showing the photodiode (diode type 2.1, red) that has been used.

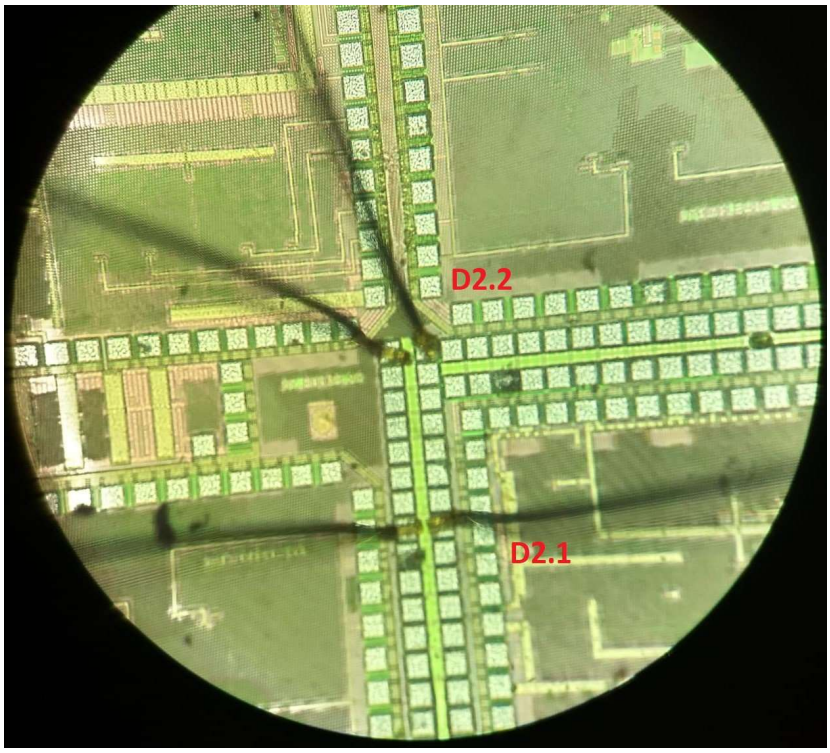

Figure 3.2: Diode type 2 seen trough microscope.

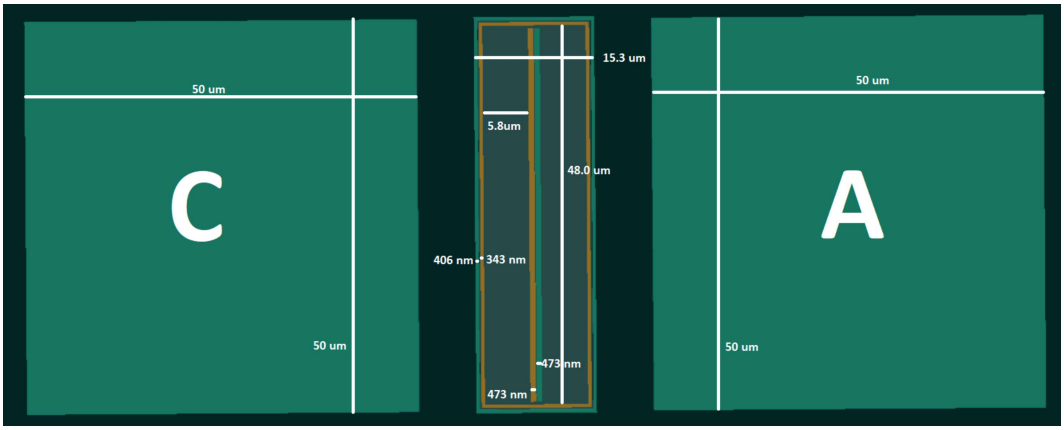

Figure 3.3: Diode type 2.1 (topview) seen by GDS3 viewer with C cathode and A anode.

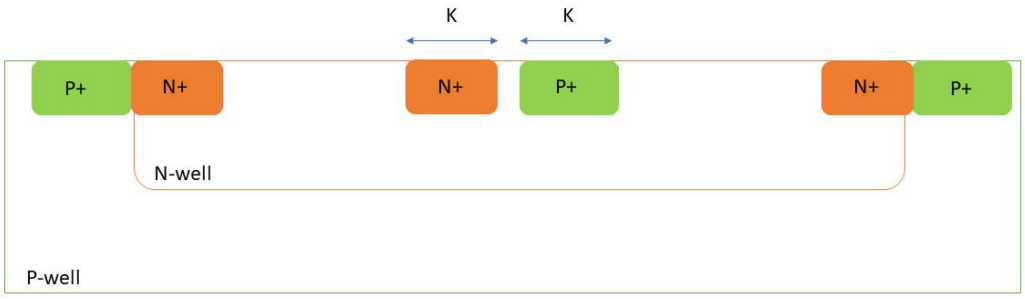

Figure 3.4: Schematic of diode type 2.1 (cross section).

In order to understand the photodiode, the I-V curve at room temperature in dark and light circumstances are presented in figures 3.5 and 3.6 for respectively the probestation and the cryostat. Both figures show some unexpected results and noise between approximately 0.0 V and -1.0 V. The probestation shows a breakdown voltage around -4.5 V and the cryostat a breakdown voltage around -3.0 V for both dark and light circumstances.

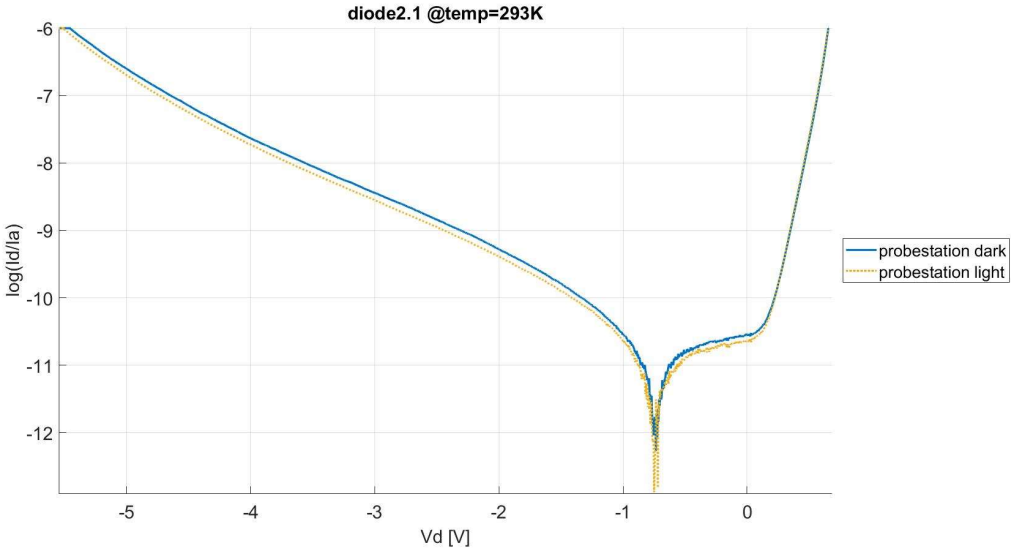

Figure 3.5: I-V curve of the diode type 2.1 in dark and light circumstances at T=293K for the probestation.

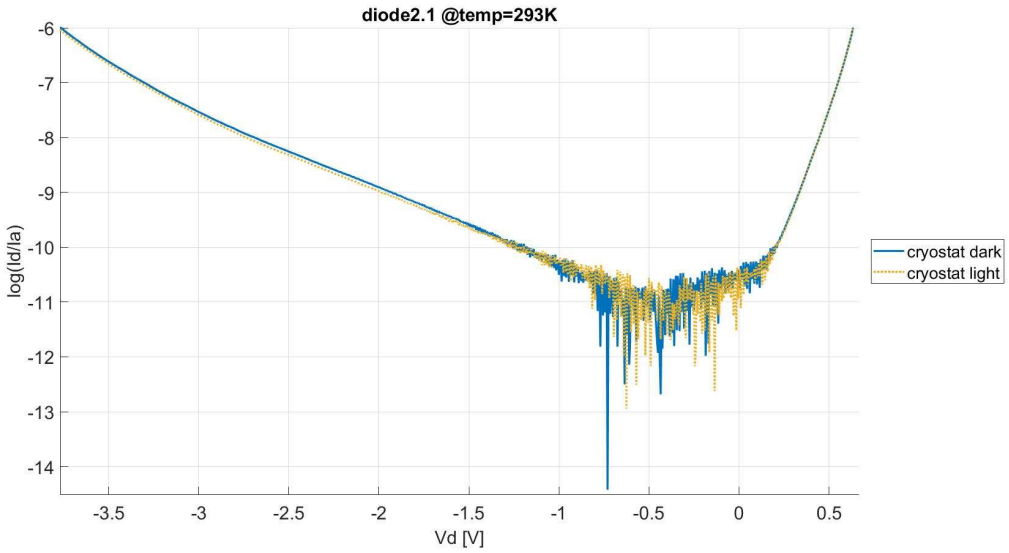

Figure 3.6: I-V curve of the diode type 2.1 in dark and light circumstances at T=293K for the cryostat.

3.2 Measurements

Parameter Analyser

In order to measure the I-V curve of the photodiode, the semiconductor characterization system 4200-SCS of Keithley was used together with the ProbeShield M300 waferprober with controlled heater/cooler ranging from 233K to 473K. The chips were mounted to sample holders (figure 3.7) with gold bondwires with the TPT HB16. This is needed for further research with the cryostat.

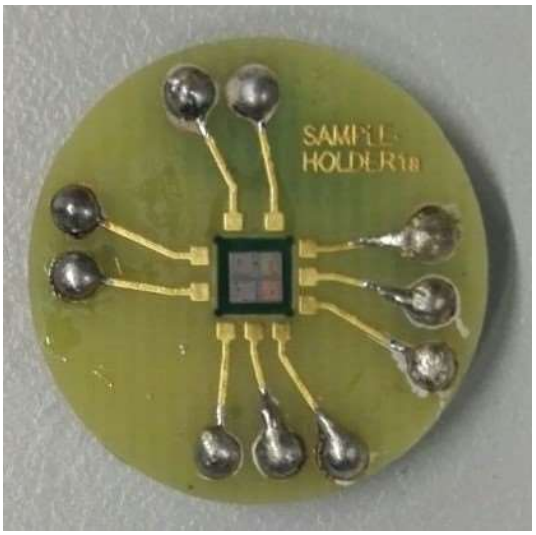

Figure 3.7: sample holder with the chip (no bonding yet).

From the measurements, various figures of merit of the conventional photodiode could be found. This could be done using equations 3.1 – 3.5 [2]. The breakdown voltage could easily be seen from the I-V curves.

$$I_{SC} = -I_L, \tag{3.1}$$

which represents the short circuit current [A] (I_{SC}) with photocurrent [A] (I_L).

$$V_{OC} = -U_T \cdot ln\left(1 + \frac{I_L}{I_o}\right), \tag{3.2}$$

which represents the open circuit voltage [V] (V_{OC}) with thermal voltage [V] U_T, photocurrent [A] I_L and reverse saturation current [A] I_o.

$$P_{MAX} = -I_o \cdot V_{MP}^2 \cdot \frac{1}{U_T} \cdot \exp\left(\frac{V_{MP}}{U_T}\right) = V_{MP} \cdot I_{MP}, \tag{3.3}$$

which represents maximum power [W] (P_{MAX}) with thermal voltage [V] U_T, reverse saturation current [A] I_o, voltage across the diode at maximum power [V] (V_{MP}) and current at maximum power [A] (I_{MP}).

$$\eta = CF \cdot \frac{V_{OC} \cdot I_{SC}}{P_{optical}}, \tag{3.4}$$

$$CF = \frac{V_{MP} \cdot I_{MP}}{V_{OC} \cdot I_{SC}}, \tag{3.5}$$

which represents the efficiency η with open circuit voltage [V] V_{OC}, short circuit current [A] I_{SC}, optical power [W] ($P_{optical}$), voltage across the diode at maximum power [V] V_{MP} and current at maximum power [A] I_{MP}.

Cryostat

The cryostat of Oxford Instruments (figure 3.8) was used for the measurements at cryogenic temperatures. The samples were attached to a holder which fits in the cryostat. The cryostat was connected to a matrix coupler, which was coupled to the parameter analyser. By changing the (cryogenic) temperature, the I-V curve variations due to low temperatures can be found.

The first measurements were done in dark conditions. Similar I-V curves were measured as before on the PM300 probestation for room temperature measurements using the same parameter analyser.

The next measurements were done using an optical set-up outside of the cryostat in front of the glass. Since the glass of the cryostat could influence the light energy, a light power meter was used to measure the light energy beforehand. Keeping the measurements in mind, the photodiodes were exposed to light while being at cryogenic temperatures. The optical measurement set-up with explanation can be found in appendix C. Again I-V curves with the same parameter analyser were measured.

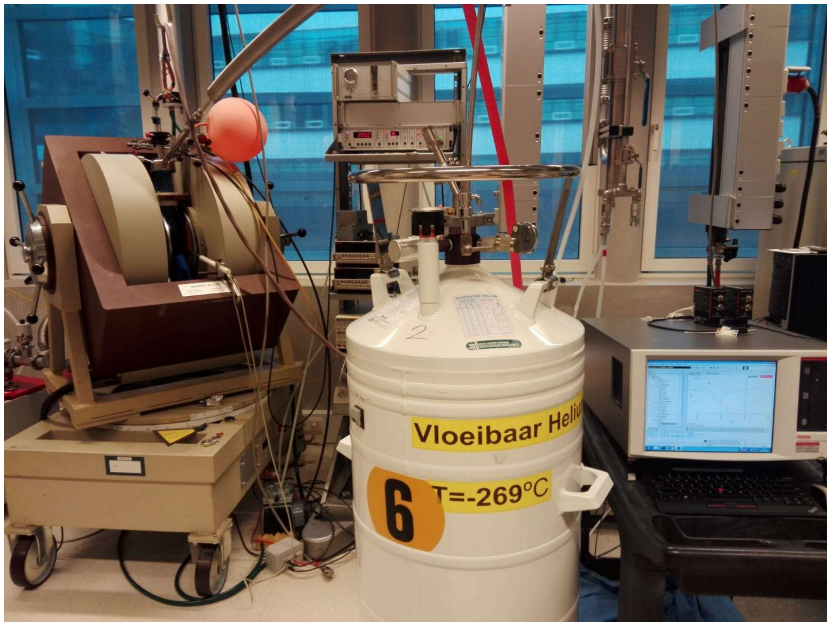

Figure 3.8: cryostat full working station.

Chapter 4

Results

The results from the electrical and electro-optical measurements are shown here. Figures 4.1, 4.7, 4.12 and 4.16 show the I-V curve with a logarithmic y-axis; figures 4.3, 4.8, 4.13; 4.17 show the full I-V curves and figures 4.4, 4.9, 4.14 and 4.18 show the I-V curve zoomed in at the breakdown region and figures 4.6, 4.11, 4.15 and 4.19 show the I-V curve zoomed in at the forward region.

4.1 Electrical measurements

Probestation

Figures 4.1 to 4.6 show the electrical photodiode measurements for diode type 2.1 with the probestation.

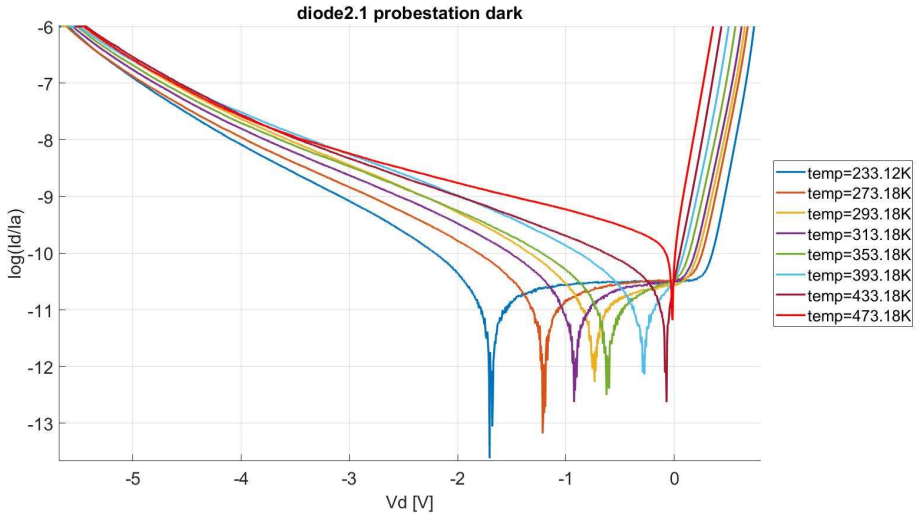

Figure 4.1: Diode type 2.1 at dark circumstances for various temperatures (see legend) in a semi-logarithmic scale.

In figure 4.1 it is visible that there is some sort of noise from 0.0 V to -2.0 V. It is noticeable that the point where the current is zero, is at negative voltages, which is not what is expected (no current, so no voltage). The forward region shows the exponential behaviour. The breakdown region shows some crossing of lines, which means that at a certain voltage, the current is higher than at another temperature. The reverse current changes in sign possibly due to the vertical diode or some parasitic

BJT caused by it. Figure 4.2 shows that not only a diode is present between the middle N+ and P+, but also via the P-well - N-well - P+.

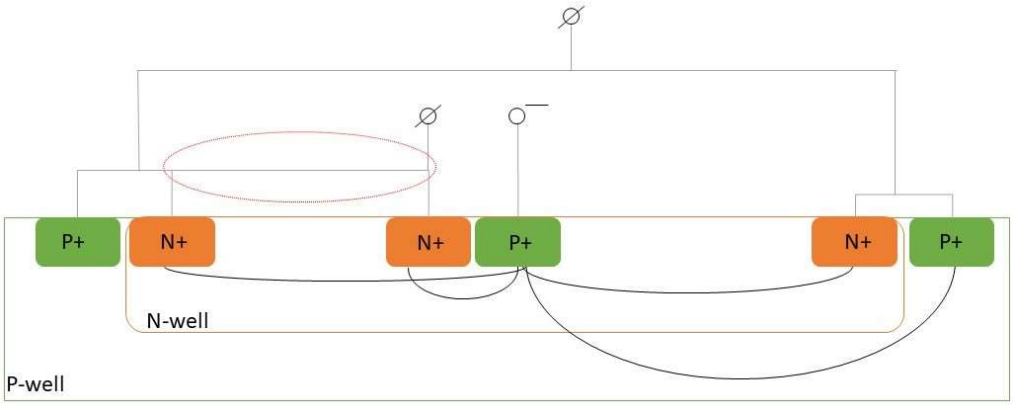

Figure 4.2: cross section of the photodiode, having various leakage currents and connections within the photodiode.

The I-V curve moves towards the y-axis with increasing temperature for the forward and breakdown region, which could be a sign of Zener effect (see chapter 2) or due to the vertical diode.

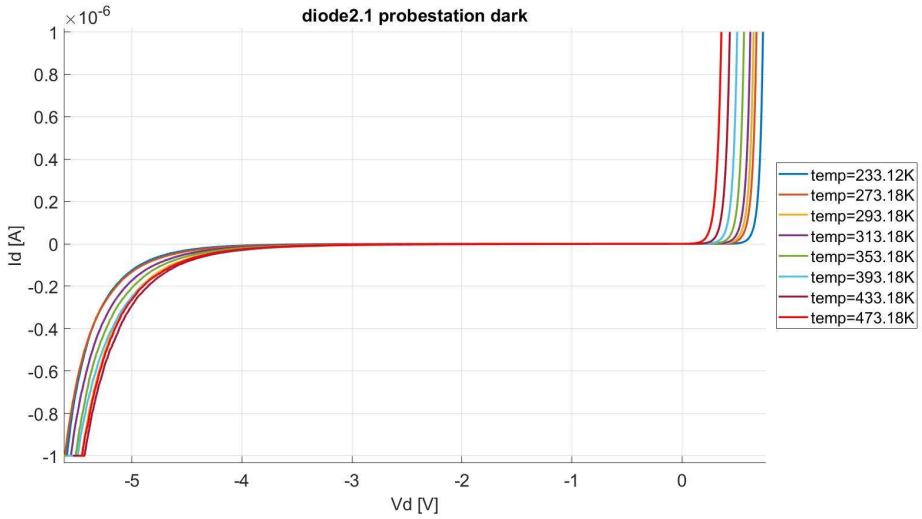

Figure 4.3: Diode type 2.1 at dark circumstances for various temperatures (see legend).

In figure 4.3 it is visible that all curves follow the same pattern. Again it is visible in the forward region how the I-V curve moves to the y-axis for increasing temperature. The breakdown region shows that the breakdown voltages lie between -4.0 V and -5.0 V.

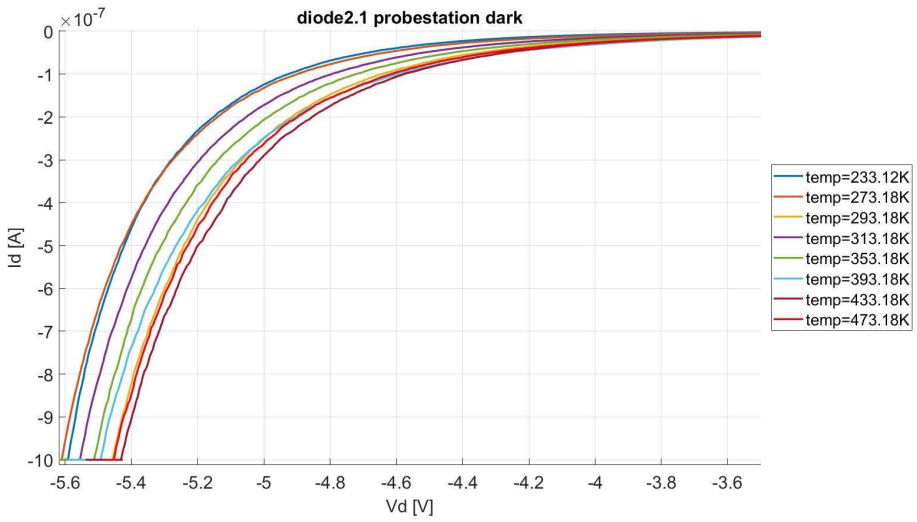

Figure 4.4: Diode type 2.1 at dark circumstances for various temperatures (see legend) zoomed in at the breakdown region.

Figure 4.4 shows the breakdown region. Here it is visible that the order of I-V curves does follow the order of temperatures. Temperatures 233.12K, 293.18K and 473.18K are not placed at their expected location (following the order of temperature). Temperatures 233.12K and 473.18K are the extreme temperatures of the probestation and could therefore be different. Another option could be the vertical parasitic diode, which could play a bigger role than before. Furthermore it is visible that an increase in temperature means a shift to the right.

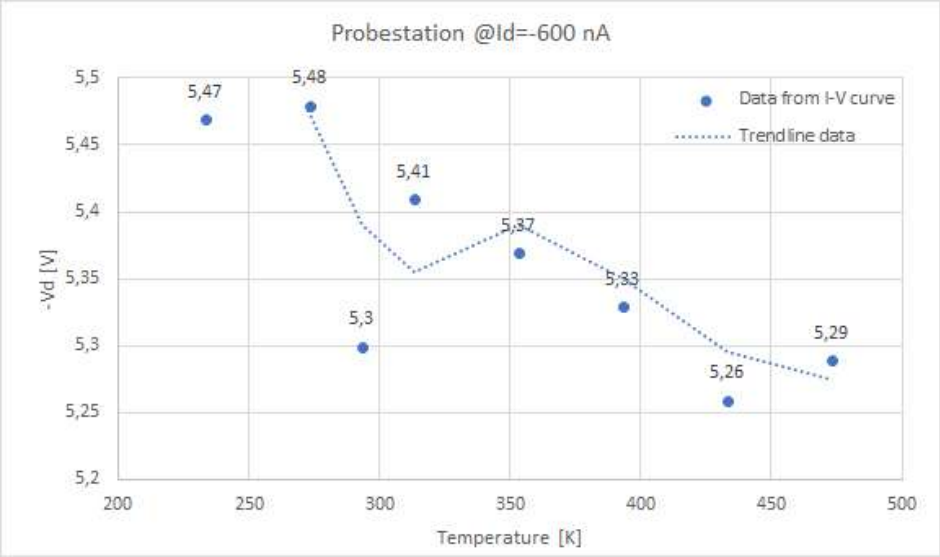

Figure 4.5: data from the I-V curve at -600 nA plotted with trendline.

Figure 4.5 shows the different voltages for Id = -600 nA of all temperatures. Here it is visible that a higher temperature leads to a lower voltage. Furthermore it is visible that 233.12K, 293.18K and 473.18K are indeed located differently from the trend.

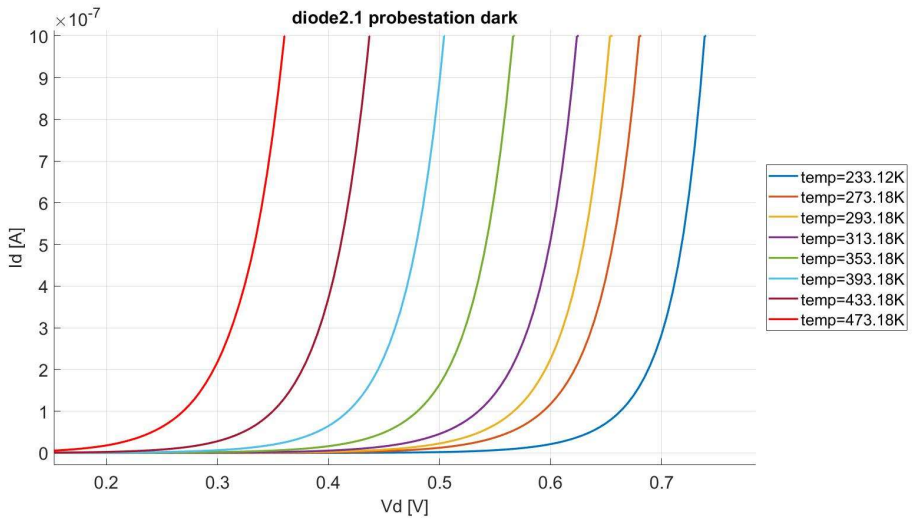

Figure 4.6: Diode type 2.1 at dark circumstances for various temperatures (see legend) zoomed in at the forward region.

Figure 4.6 shows the forward region of the I-V curve. Here the temperature dependence is clearly visible: a higher temperature moves the I-V curve towards the y-axis. The noise visible above 0 A, will be explained later.

Cryostat

Figures 4.7 to 4.11 show the electrical photodiode measurements for diode type 2.1 with the cryostat.

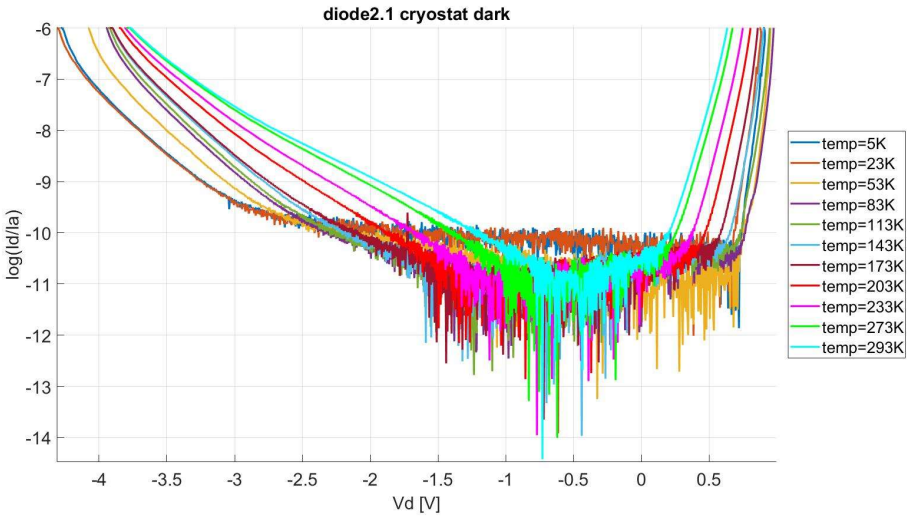

Figure 4.7: Diode type 2.1 at dark circumstances for various temperatures (see legend) in a semi-logarithmic scale.

Figure 4.7 shows the semi-logarithmic scale I-V curve for the cryogenic measurements. Here, noise is visible between approximately -3.0 V and +0.6 V. Furthermore, breakdown is visible between -4.5 V and -3.5 V and the forward region shows an exponential behaviour.

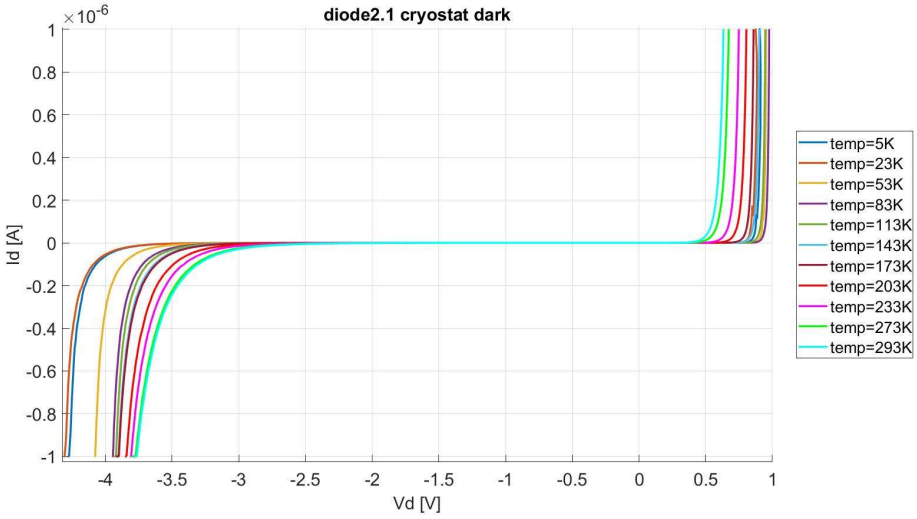

Figure 4.8: Diode type 2.1 at dark circumstances for various temperatures (see legend).

Figure 4.8 shows the same behaviour as in figure 4.3. Both the forward region shows non consistency in the lines with temperatures 5K and 23K, but these are the extreme temperature. This could be a measurement device error or an effect on the ultra low temperatures.

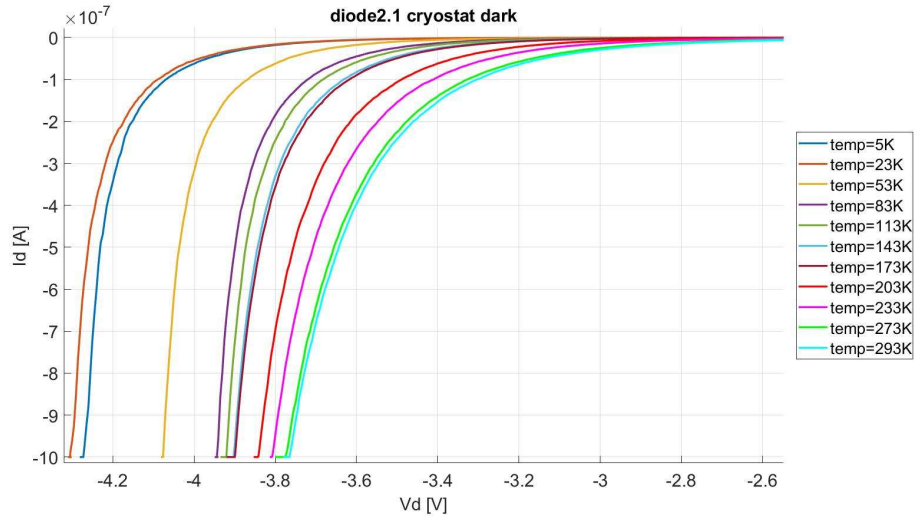

Figure 4.9: Diode type 2.1 at dark circumstances for various temperatures (see legend) zoomed in at the breakdown region.

The breakdown region in figure 4.9 shows that the I-V curve moves towards the y-axis for higher temperatures. The two odd temperatures are 5K and 23K, which are switched according to their expected location (based on the order of temperatures). This could be due to the Zener effect or by the vertical diode.

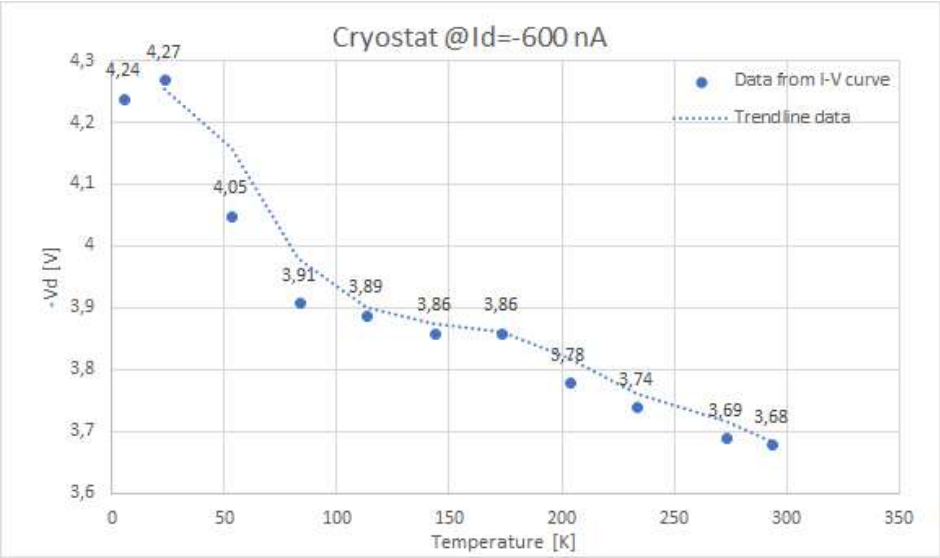

Figure 4.10: data from the I-V curve at -600 nA plotted with trendline.

Figure 4.10 shows the different voltages for Id = -600 nA of all temperatures. Here it is visible that a higher temperature leads to a lower voltage. Furthermore it is visible that 5K and 23K are indeed located differently from the trend.

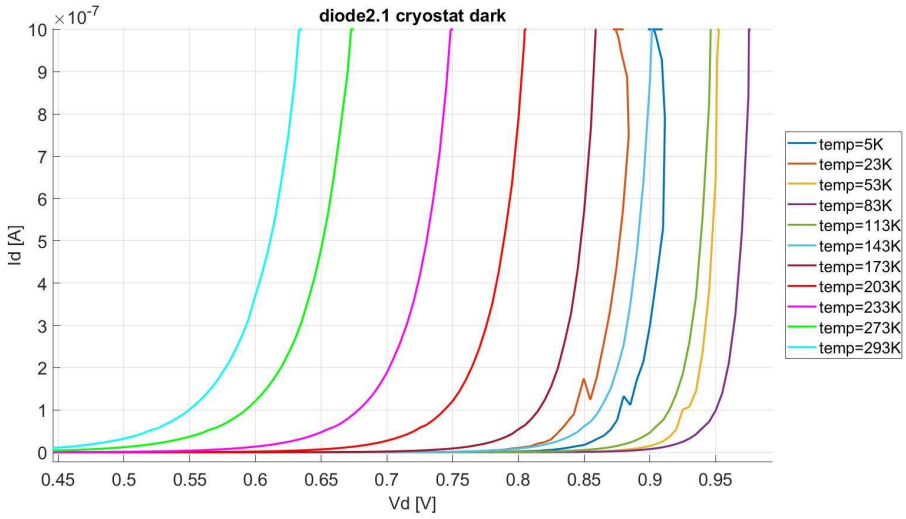

Figure 4.11: Diode type 2.1 at dark circumstances for various temperatures (see legend) zoomed in the forward region.

The forward region in figure 4.11 shows that 5K, 23K and 53K have inconsistencies and are not showing the expected trend (ordered on temperature). However, these are also the extreme temperatures. The other temperatures are placed as they were expected, moving towards the y-axis for higher temperatures. The odd behaviour for 5K, 23K and 53K could be due to a measurement device error or due to behaviour at ultralow temperatures.

4.2 Electro-optical measurements

Probestation

Figures 4.12 to 4.15 show the electro-optical photodiode measurements for diode type 2.1 with the probestation.

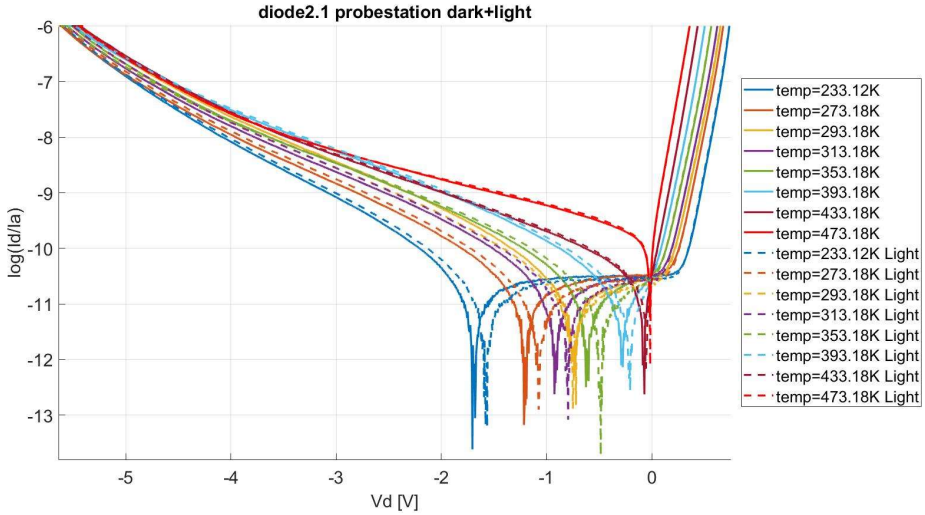

Figure 4.12: Diode type 2.1 at light circumstances for various temperatures (see legend) in semi-logarithmic scale.

Figure 4.12 shows the circumstances in dark and in light. The forward region does not show significant change with or without light. The breakdown region shows some reaction to the light, but this is also minimal. Again noise can be found between -2.0 V and 0.0 V.

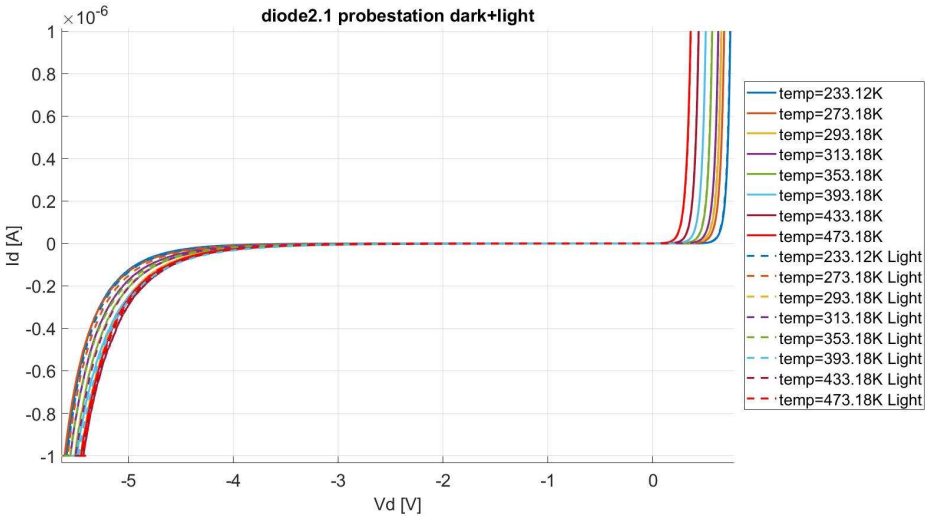

Figure 4.13: Diode type 2.1 at light circumstances for various temperatures (see legend).

Figure 4.13 shows the I-V curves. The forward region again shows almost no reaction to light. The breakdown region shows some reaction towards the light. The breakdown voltage is between -4.0 V and -5.0 V.

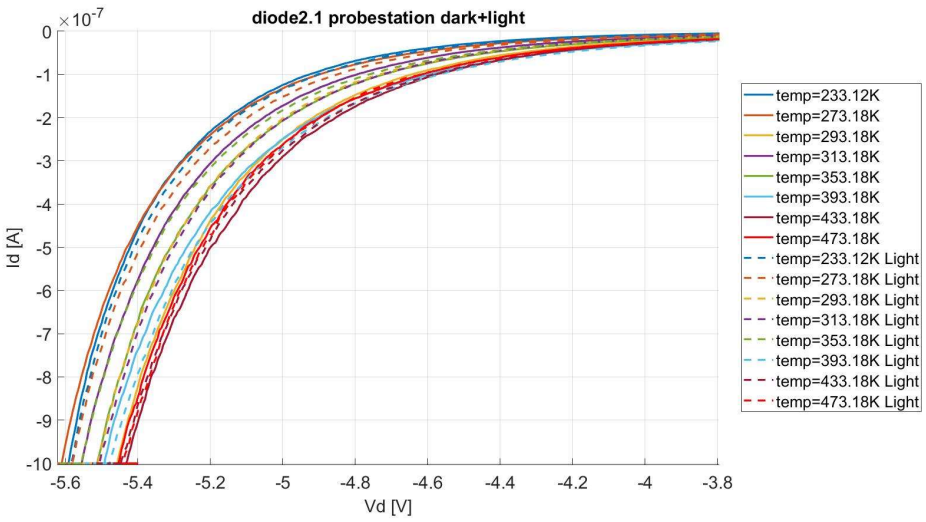

Figure 4.14: Diode type 2.1 at light circumstances for various temperatures (see legend) zoomed in at the breakdown region.

The breakdown region in figure 4.14 is between approximately -4.0 V and -5.0 V. Temperatures 394.18K, 353.18K and 433.18K show a different behaviour for temperature. Here, the I-V curve of light is above the corresponding I-V curve of dark. Again limited reaction to light is visible. This could be due to the Zener diode or the vertical diode does not react to light and is electrically dominant for the total current.

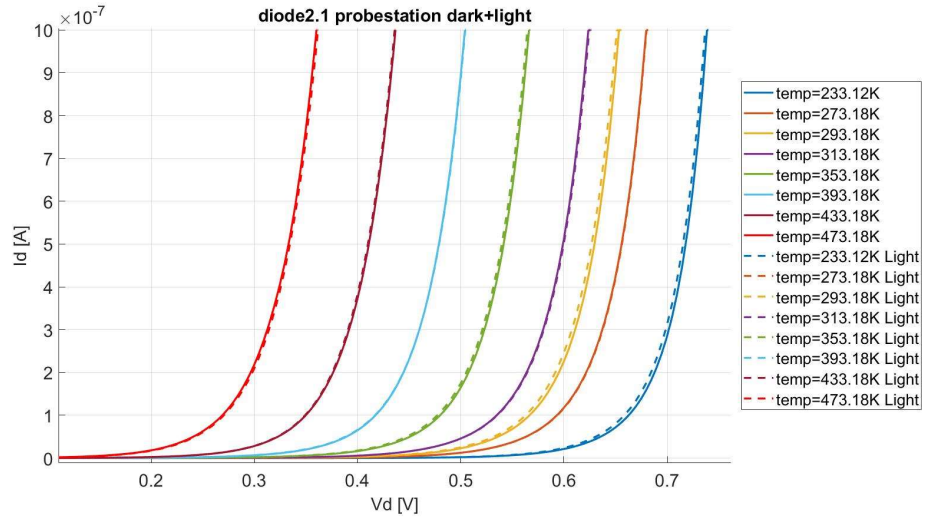

Figure 4.15: Diode type 2.1 at light circumstances for various temperatures (see legend) zoomed in at the forward region.

The forward region in figure 4.15 shows limited till no reaction to light. However, the temperature relation still holds.

Cryostat

Figures 4.16 to 4.19 show the electro-optical photodiode measurements for diode type 2.1 with the cryostat.

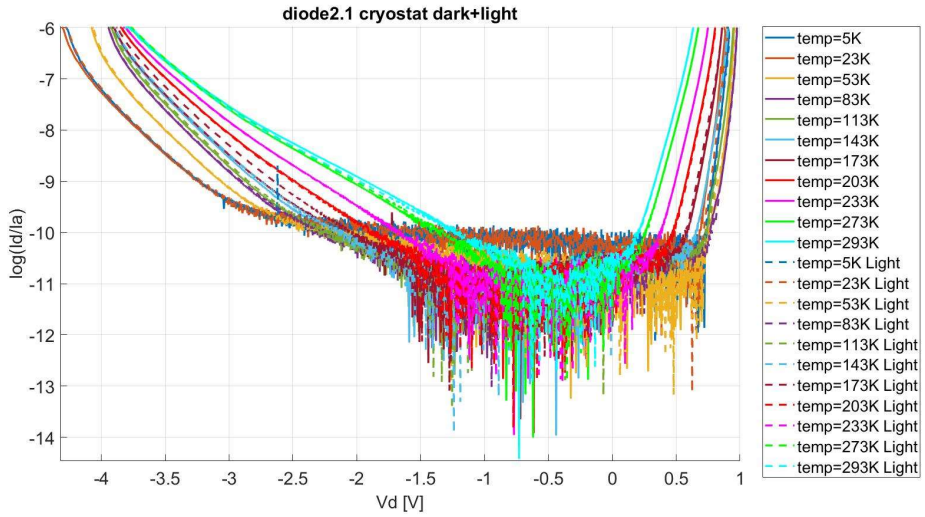

Figure 4.16: Diode type 2.1 at light circumstances for various temperatures (see legend) in semi-logarithmic scale.

Figure 4.16 shows the circumstances of dark and light with the I-V curve. Again, lots of noise can be found between approximately -3.0 V and +0.7 V. Again, limited to no reaction to light can be found in the forward and breakdown region.

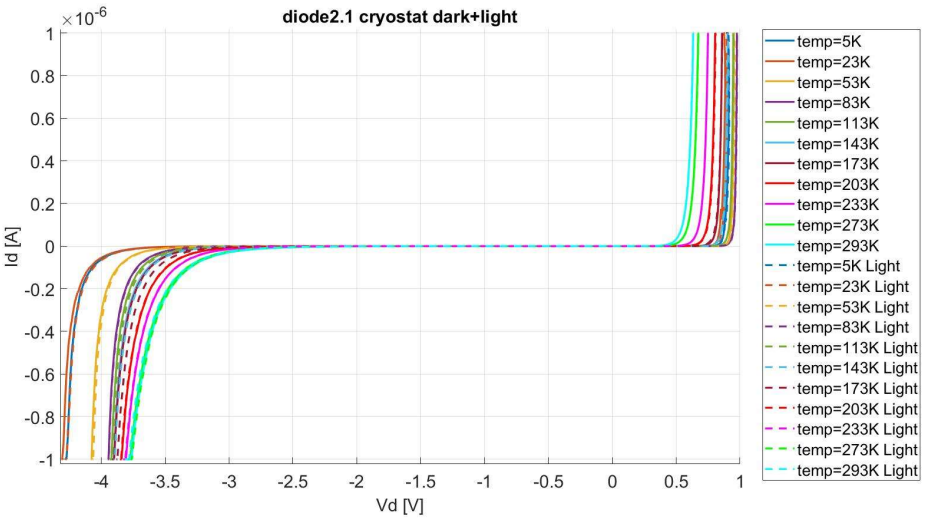

Figure 4.17: Diode type 2.1 at light circumstances for various temperatures (see legend).

Figure 4.17 shows the expected curvature of the I-V curve. The breakdown voltages are approximately between -3.0 V and -4.0 V. Limited reaction to light can be found in the figure.

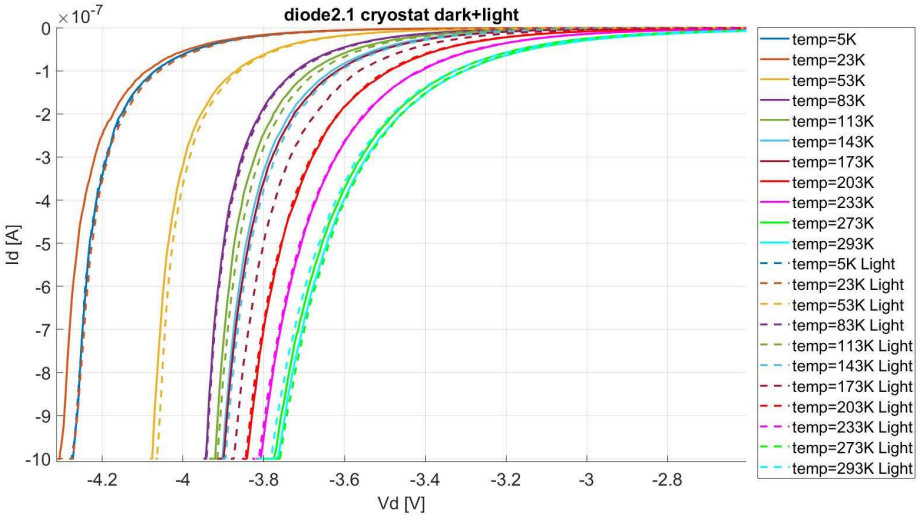

Figure 4.18: Diode type 2.1 at light circumstances for various temperatures (see legend) zoomed in at the breakdown region.

The breakdown region in figure 4.18 again shows some odd figures for temperatures 293K, 233K and 203K. Here, the light I-V curve is higher then the dark I-V curve, which is not what is expected for a photodiode. Repeatedly, almost no reaction to light is visible.

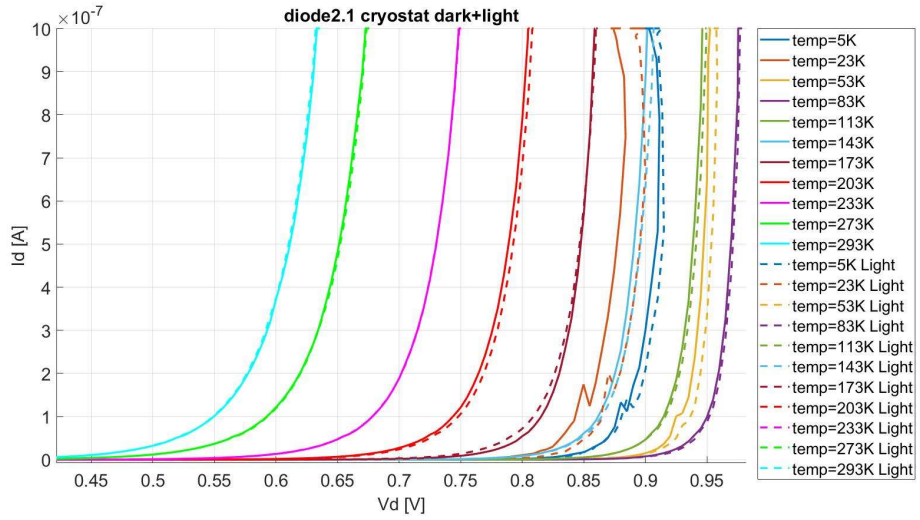

Figure 4.19: Diode type 2.1 at light circumstances for various temperatures (see legend) zoomed in at the forward region.

The forward region in figure 4.19 shows the same inconsistencies as in figure 4.11. The lower temperatures, starting from 203K, show more reaction to light than the highest three temperatures. However, the behaviour shown is again not what is expected for photodiodes (see chapter 2). The light curve should be below the dark curve, which is the case. The odd behaviour for 5K, 23K and 53K could be due to a measurement device error or due to behaviour at ultralow temperatures.

Chapter 5

Discussion

The results in chapter 4 gives for now two hypotheses for the odd behaviour: the Zener effect could play an important role; the vertical parasitic diode plays a more important role than expected. A combination of both is also possible. In this chapter, both options are discussed.

The results in chapter 4 show that the breakdown voltage will move towards 0 V for higher temperatures. This is not the expected outcome for a conventional or avalanche photodiode, but is what one would expect for a Zener diode (see chapter 2). This could also explain why the photocurrent is not lower when a light source is exposed to the photodiode compared to the photocurrent without a light source. However, the vertical diode could also dominate, which is also insensitive to light due to the vertical position. This could be due to the depletion width of the Zener diode, which is relatively small compared to the conventional photodiode. When the depletion width is relatively small, limited amount of photons can be captured. Seeing equation 5.1 [2],

$$I_{\mathrm{L}} = \frac{\eta \cdot q \cdot A \cdot I_{\mathrm{illum.}}}{h \cdot v} = \frac{\eta \cdot q \cdot A \cdot I_{\mathrm{illum.}} \cdot \lambda}{h \cdot c}, \tag{5.1}$$

the area is small, so I_L is close to zero and therefore, almost no change in I_D can be seen. Combining these results and knowing that the diode is highly doped and the p and n region are close to each other, it is likely that the photodiode is a Zener diode.

On the other hand, S. Dutta et al. state in the paper [20] that the Zener effect is visible for diodes of approximately 60 nm or smaller width between the p and n region. In this case, this distance is 100 nm, which should be sufficient.

From the measurements, it is also visible that the 5K and 23K and the 433K and 473K I-V curves are switched compared to what is expected. A reason for the 5K and 23K could be that the avalanche breakdown takes over in the diode, causing an earlier breakdown. As already stated in chapter 2, a Zener diode works with three regions: the Zener effect, the avalanche breakdown and a combination of both [9], [10]. This combination varies in ratio depending on the voltage and temperature. Also, the doping will not work efficiently at low temperatures. For Si, this will be below approximately 100K [1], [14]. The internal electric field will decrease in strength, meaning that the Zener effect will decrease as well. Moreover, the tunneling probability [9] is approximately

$$Z \approx \exp(\frac{-\alpha E_{\mathrm{g}}^{\frac{3}{2}}}{\mathrm{F}}), \tag{5.2}$$

with tunneling probability (Z), tunneling probability variable (α) and field strength (F), where it is visible that the probability is dependent on the band gap energy. Since the band gap energy increases

slowly for decreasing temperatures, the probability will decrease as well [9]. When the probability of tunneling decreases, the avalanche breakdown becomes more dominant. The opposite could be true for 433 K and 473K, where the Zener breakdown could become dominant.

Furthermore, it is visible that breakdown voltages, for the same temperature, differ for the probestation and the cryostat. This is most likely due to a systematic error in the probestation and/or the cryostat. Since frosting will most likely develop on the chip for colder temperatures, this could influence the measurement. The frosting has been detected on the chip for the measurements with the probestation. For the cryostat, it could not be seen whether this was the case as well.

Another option could be the order of cooling down/warming up. It is very likely that trap assisted tunneling (TAT) occurs in this diode. This could mean that when the measurements start at higher temperatures, electrons could be stored on these traps. When the diode is then cooled down, these electrons still have the opportunity to move from the traps. This process is temperature dependent due to the Fermi-tail, which is visible in figure 5.1. However, this is not the wanted effect to measure.

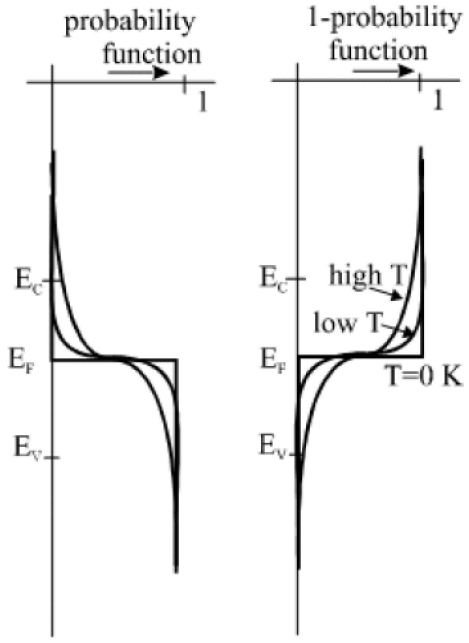

Figure 5.1: Fermi tail probability function and 1-probability function [11].

The traps could also help Shockley-Read-Hall (SRH) recombination [14]. This process is the dominant generation and recombination process in lightly doped silicon pn-junctions due to the indirect band gap. The energy is exchanged in the form of phonons.

Phonons are also needed for the Zener effect due to the indirect band gap. Since the lattice will stand still for 0K, there will be no phonons. So the SRH recombination, Zener effect and TAT become less important at lower temperatures. Meaning again that the avalanche breakdown becomes more dominant, where possibly more direct transitions are possible.

Lastly, the photodiode shows a lot of noise in the middle region (between avalanche and forward region). This could come from the Zener diode, which is known to have relatively high electronic noise [13]. However, it could also be a combination with another noise source, like the vertical diode, or another noise source. The P-well and N-well could also give some suspicious leakage currents, most likely due to the connected encircled P-N junction, the guard ring, which is also visible in figure

5.2. Unfortunately, the parasitic current will not be constant for every temperature.

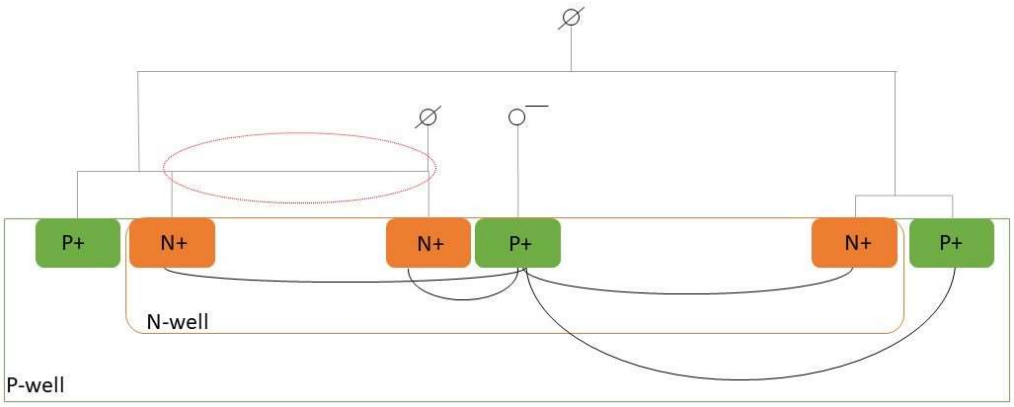

Figure 5.2: cross section of the photodiode, having various leakage currents and connections within the photodiode.

Since the measurements showed noise, four different measurement were done to investigate to this. First the noise through the air (blue in figure 5.3) is measured, which is also the noise of the PM300. This has been done by lifting both probes and do a measurement. Second a sample holder with a not bonded chip has been measured in light (red in figure 5.3) and dark circumstances (orange in figure 5.3). Last, a sample holder without chip has been measured (purple in figure 5.3).

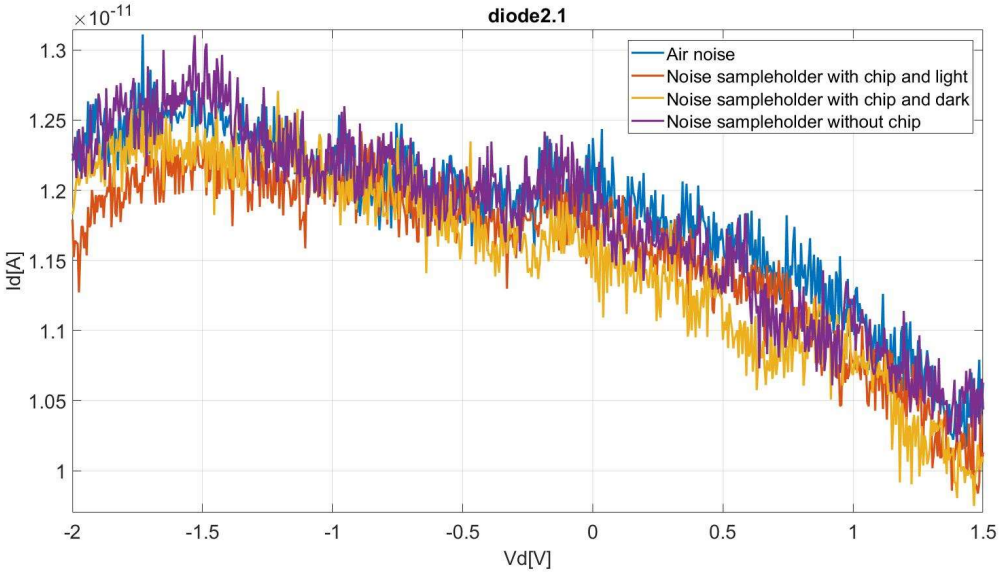

Figure 5.3: Noise measured in air; sample holder with chip and light; sample holder with chip and dark and sample holder without chip.

It is visible that the sample holder with and without chips gives noise of around 10 pA.

Furthermore, the chip that is bonded to the sample holder is compared to two unbonded chips measured with the probestation. The results for 293K and 473K can be found in figures 5.4 and 5.5 respectively.

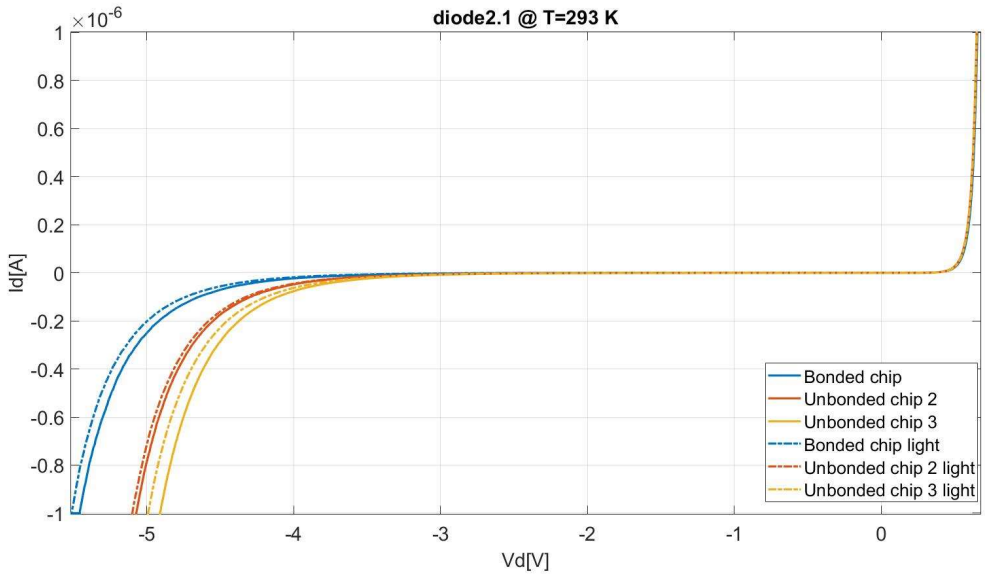

Figure 5.4: Diode bonded and twice unbonded with and without light at T=293K.

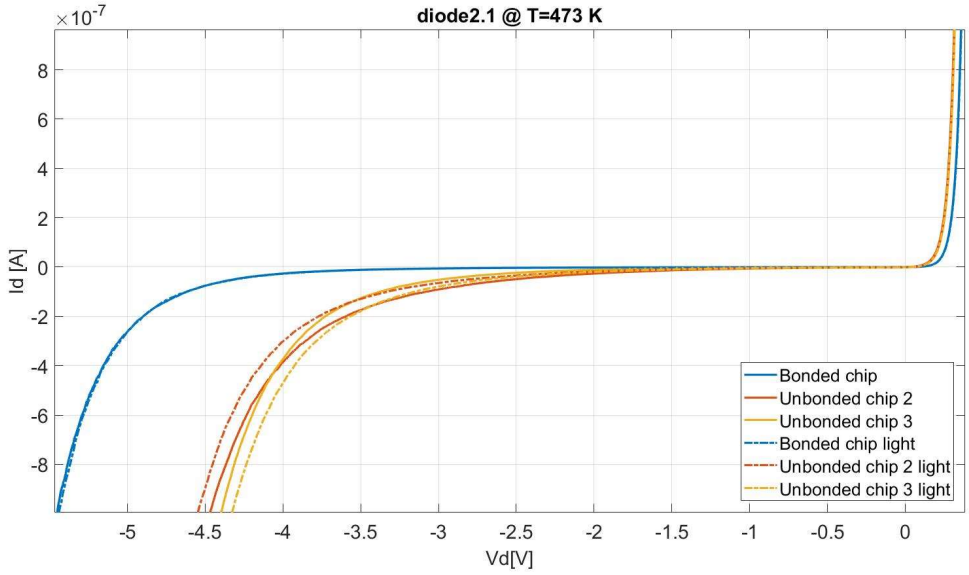

Figure 5.5: Diode bonded and twice unbonded with and without light at T=473K.

Figures 5.4 and 5.5 show that the breakdown voltage is lower for the unbonded chips then for the bonded chip. Moreover, the bonded chip shows less change in the breakdown voltage for the temperature difference compared to the unbonded chips. This difference could come from the bonding. However, it is also visible that the two unbonded diodes also have a different breakdown voltage. Therefore, more circumstances could play a role during measurements like the humidity and noise from the wafer or sample holder.

Chapter 6

Conclusions and recommendations

This chapter consists of two sections. The first section is the conclusion on the research explained in this report. The second section shows the recommendations.

6.1 Conclusions

The research started with the two sub research questions:

1. What is the influence of the temperature on the breakdown voltage of silicon photodiodes?
2. What is the influence of light on the breakdown voltage of silicon photodiodes at cryogenic temperatures?

leading to the main research question, *What is the influence of temperature on light detection in silicon photodiodes?*.

Unfortunately, these research question have a different meaning when a Zener diode is used. The negative temperature coefficient of the Zener diode showed to be true, but the avalanche breakdown seems to dominate at extremely low temperatures. The relatively small depletion region of the Zener diode or the insensitivity of the vertical diode made that there was limited to no light absorption, so no conclusion about that could be found. Since the second sub question could not be answered, given this Zener diode, the main research question can also not be answered.

6.2 Recommendations

From this research, the temperature relations for the (Zener) diodes used needs to be analysed in more detail. Although this research was about cryogenic temperature and light, it became clear that still a lot is unknown about the temperature effects on (Zener) diodes. More research on this topic is needed in order to fully understand the behaviour of the diodes.

Additionally, analysis on how photodiodes react to light at cryogenic temperatures needs to be done more. This research was a small step towards more investigation on this topic. Knowing these results, more accurate and intense research is needed to apply the results to the various applications.

Similarly, analysis on what type of photodiode could be the best fit for this specific circumstance is needed. Since the photodiodes used during this research were not the best fit to the circumstances, better results could be found when the diodes would fit. These circumstances are cryogenic temperatures and sizes suitable for analysis.

Furthermore, the responsivity of Si photodiodes at cryogenic temperatures could be analysed more. For this research, it could not be researched properly whether the responsivity would change dramatically at cryogenic temperatures for specific wavelengths, while it is expected that there would be an abrupt end at higher wavelengths.

Moreover, research on Zener effects which can be used for near infrared (NIR) detection could be analysed more. More about this also in Near-Infrared Detection Using Pulsed Tunneling Junction in Silicon Devices of H. Kim et al. [21].

This research could be improved in several ways. The main problem was the bonding of the chip to the sample holder, since the bondpads of the diodes were only 50 microns big. This made the bonding overlap with other bondpads, causing shorts and parallel measurements. In the future, this could be solved by designing the diodes in such a way that there is enough space around the bondpad to disperse or larger bondpads.

Likewise, some active area of the photodiodes had been covered with gold of the wirebond which caused less till no light absorption. This could easily be improved by changing the bondpads.

Furthermore, the design of the photodiode, as is visible in figure 5.2, should be improved. The photodiode is a P-N junction with guard ring. This encircled P-N junction is connected to the N+ of the intended photodiode. This means that not one but two diodes are measured, with probably each their own characteristics. This could easily be solved when redesigning the photodiodes by not connecting both the N+'s (leaving out the red dotted encircled line in figure 5.2 in chapter 5).

The diodes themselves should be changed. The doping should be lowered, such that no Zener diodes are fabricated. A p+/n-/n+ or p+/p-/n+ diode with n-/p- spacing of at least 0.5 μm spacing could be a good option [20].

Moreover, the measurement set-up still showed some sort of noise. This noise is most likely from the diode design with the p-n junction encircled with another p-n junction. Due to this, parasitic currents which are dependent on temperature occur. Due to limited time, this noise could not be researched on any further. However, this noise does influence the photodiode. Therefore, a closer look to the noise is needed in the further to improve this research.

Additionally, the research could be performed with more accuracy. The temperature steps in this research were 40 degrees per step. When having smaller steps, the accuracy could be improved. In addition, the full measurements should be performed multiple times to cover any measurement and circumstantial errors.

The optical set-up also did not work as planned. The set-up had to be made with limited time and knowledge. Luckily, with help, the set-up could be designed and built. However, at the final step, the light intensity was not enough and the amount of extra light from the room of the cryostat was too much. This could have been solved when spending more time in the optical set-up. Also moving the cryostat to an optical lab which is without light would be favored.

Equally important, the power of the light in the cryostat has not been measured. Therefore it is unknown what the glass of the cryostat does to the light and how much power has been exposed to the diode. A measurement with a power meter could solve this.

Finally, much time was lost during the research. During measurements this was due to switching of SMUs. Since 2 out of 4 SMUs were connected to an amplifier with specific settings, the 2 SMUs that were suitable for measurements needed to switch between the two diodes that were measured at the same sample holder. When four SMUs had had worked, this could have saved time and therefore result in more measurements with smaller temperature steps. Likewise waiting for the bonding of the chips resulted in less time for measurements. This resulted in less accuracy in the measurements.

List of abbreviations and symbols

IDS	Integrated Devices and Systems
ICD	Integrated Circuit Design
NE	NanoElectronics
UT	University of Twente
APD	avalanche photodiode
Si	silicon
SRH	Shockley-Read-Hall
TAT	trap assisted tunneling
NIR	near infrared
SCS	semiconductor characterization system

c	speed of light $= 3.00 \cdot 10^{10}\ [\frac{\mathrm{cm}}{\mathrm{s}}]$
h	Planck's constant $= 6.63 \cdot 10^{-34}\ [\mathrm{J} \cdot \mathrm{s}]$
q	elementary charge $= 1.6 \cdot 10^{-19}\ [\mathrm{C}]$
k	Boltzmann constant $= 1.38 \cdot 10^{-23}\ [\frac{\mathrm{J}}{\mathrm{K}}]$
$E_g(0)$	band gap energy at 0 Kelvin $= 1.170\ [\mathrm{eV}]$ [15]
α	silicon bandgap specific constant $= 4.730 \cdot 10^{-4}\ [\frac{\mathrm{eV}}{\mathrm{K}}]$
β	silicon bandgap specific constant $= 636\ [\mathrm{K}]$
I_a	mathematical constant $= 1\ [\mathrm{A}]$

V_b	break-down voltage [V]
V_D	voltage across the diode [V]
U_T	thermal voltage [V]
V_{OC}	open circuit voltage [V]
V_{MP}	voltage across the diode at maximum power [V]

I_o	reverse saturation current [A]
J_0	reverse saturation current density [$\frac{\mathrm{A}}{\mathrm{m}^2}$]
I_L	photocurrent [A]
$I_{illum.}$	intensity of illumination [$\frac{\mathrm{W}}{\mathrm{cm}^2}$]
I_{SC}	short circuit current [A]
I_{MP}	current at maximum power [A]
T	temperature [K]
E_g	band-gap energy [eV]
α	absorption coefficient [$\frac{1}{\mathrm{cm}}$]
λ	wavelenght of light [μm]
v	frequency of photon [Hz]
n	ideality factor
ε	electric field [$\frac{\mathrm{V}}{\mathrm{cm}}$]
ρ	charge density [$\frac{\mathrm{C}}{\mathrm{cm}^3}$]
ϵ_s	permittivity [$\frac{\mathrm{F}}{\mathrm{cm}}$]
x	distance in the n layer
W	width of the n layer
A	active photodiode area [cm^2]
n_i	intrinsic carrier concentration [cm^{-3}]
N_A	doping concentration acceptor [cm^{-3}]
D_n	diffusion coefficient electron [$\frac{\mathrm{cm}^2}{\mathrm{s}}$]
L_n	length of n layer [cm]
N_D	doping concentration donator [cm^{-3}]
D_p	diffusion coefficient hole [$\frac{\mathrm{cm}^2}{\mathrm{s}}$]
L_p	length of p layer [cm]
N_C	conduction band effective density-of-states [cm^{-3}]
N_V	valence band effective density-of-states [cm^{-3}]
η	quantum efficiency
$P_{optical}$	optical power [W]

R_{lambda}	responsivity [$\frac{\mathrm{A}}{\mathrm{W}}$]
P_{MAX}	maximum power [W]
P	input power [W]
Z	tunneling probability
α	tunneling probability variable
F	field strength
Θ_m	exit angle with respect to the grating normal [°]
Θ_i	angle of the normal of the grating with respect to the incident angle of exit [°]
Θ_t	total angle between incident angle and the exit bundle of the order of interest$= 105[^\circ]$
a	grating period derived from the grating density$= 1.67[\mu\mathrm{m}]$
m	order of the wavelength of interest
Db	diameter of the light bundle [mm]
D	distance between slit and lens [mm]

Bibliography

[1] S. Sze and K. K. Ng, *Physics Of Semicondutctor Devices, third edition*. Wiley-Interscience, 2007.

[2] "Manual for the photodiode project," University of Twente, December 2014.

[3] S. Radovanovi, "High-speed photodiodes in standard cmos technology," PhD thesis, Enschede, 2004.

[4] Hamamatsu, *Opto-semiconductor handbook*. Hamamatsu. [Online]. Available: https://www.hamamatsu.com/resources/pdf/ssd/e03_handbook_si_apd_mppc.pdf

[5] L. W. Snyman, M. du Plessis, and E. Belloti, "Photonic transitions (1.4 ev-2.8 ev) in silicon p+np+ injection-avalanche cmos leds as function of depletion layer profiling and defect engineering," IEEE Journal of Quantum Elcetronics, vol. 46, no 6, June 2010.

[6] A. Gallivanoni, I. Rech, and M. Ghioni, "Progress in quenching circuits for single photon avalanche diodes," IEE transactions on nuclear science, vol. 57, no. 6, Dec 2010.

[7] C. Zener, "A theory of the electrical breakdown of solid dielectrics," PROC.R.Soc, VOL. 145, pp. 523–529, December 1933.

[8] L. Esaki, "Discovery of the tunnel diode," IEEE Transactions on Electron Devices, pp. 644–674, August 1976.

[9] M. S. Tyagi, "Zener and avalanche breakdown in silicon alloyed p-n junctions ii, effect of temperature on the reverse characteristics and criteria for distinguishing between the two breakdown mechanisms," Solid-State Electronics Pergamon Press. Vol. 11, pp. 117-128., 1968.

[10] H. Weinerth, "Silicon diode breakdown in the transition range between avalanche effect and field emission," Solid-State Electronics Pergamon Press. Vol. 10, pp. 1053-1062., 1967.

[11] R. Hueting, A. Mouthaan, and G. Sasse, "Semiconductor devices explained more," Semiconductor Systems Group, University of Twente, April 2013.

[12] G. A. M. Hurkx, D. B. M. Klaassen, and M. P. G. Knuvers, "A new recombination model for device simulation including tunneling," IEEE Transactions on Electron Devices, VOL. 39, NO. 2, February 1992.

[13] R. C. Dorf and et al., *The Electrical Engineering Handbook*. CRC Press LLC, 2000. [Online]. Available: http://hguywilliams.net/images/documents/library/Elec/dee.pdf

[14] R. F. Pierret, *Advanced Semiconductor. Fundamentals, second edition*. Pearson, vol. 6. [Online]. Available: https://pdfs.semanticscholar.org/7083/f933672d6f4b31b93b2663a183fb1a721b81.pdf

[15] D. Wolpert and P. Ampadu, *Managing Temperature Effects in Nanoscale Adaptive Systems*. Springer, 2012.

[16] C. L. F. Ma, M. J. Deen, L. E. Tarof, and J. Yu, "Modelling of breakdown voltage and its temperature dependence in sagcm inp/ingaas avalanche photodiodes," *IEEE*, Dec. 1994.

[17] S. A. E. Ahmed and M. D. Abd-Alla, "Responsivity of silicon photodiodes light and dark current under influence of different magnetic flux intensity and temperature." Journal of Applied and Industrial Sciences, Dec. 2013.

[18] B. Baker, "Collecting light power: voltaic or conductive?" October 2012.

[19] O. optoelectronics, "Photodiode characteristics and applications." [Online]. Available: http://www.osioptoelectronics.com/application-notes/an-photodiode-parameters-characteristics.pdf

[20] S. Dutta, G. J. M. Wienk, R. J. E. Hueting, J. Schmitz, and A.-J. Annema, "Optical power efficiency versus breakdown voltage of avalanche-mode silicon leds in cmos," IEEE Electron Device Letters, VOL. 38, NO. 7, July 2017.

[21] H. Kim, S. Choi, N. Yoo, M. J. Lee, and Y. J. Park, "Near-infrared detection using pulsed tunneling junction in silicon devices," IEEE Transactions on Electron Devices, VOL. 63, NO. 1, JANUARY 2016.

[22] "De monochromator fysica 2 practicum," Technologiecampus De Nayer, April 2015.

Appendix A

Chip data

A.1 Diode types

Figure A.1, A.10 and A.21 show the layout (topview) in GDS3D of respectively diode type 1, 2 and 3. The green in the GDS3D views is the p type region and the orange is the n type region. Diode 1.1, 2.1 and 3.1 have a smaller p region and n region compared to 1.2, 2.2 and 3.2. Furthermore, the diode is highly doped and the STI is not clear silicon-dioxide. Lastly, the photodiode viewed through a microscope the first measurements with the probestation can be found.

A.1.1 Diode type 1

Diode type 1 can be found in figure A.1. In this type, the distance d of the STI (found in figure A.2), increases. This means that type 1 has the smallest d and type 2 has the biggest d.

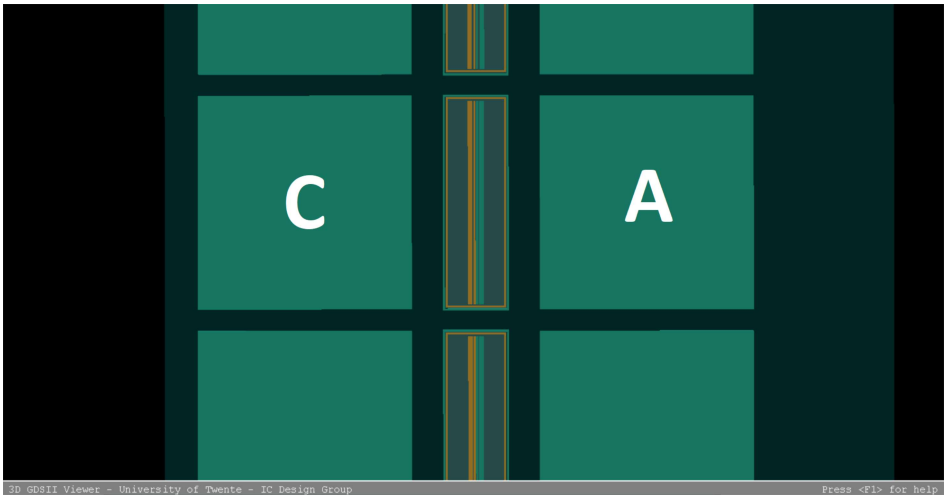

Figure A.1: Diode type 1 (topview) seen from GDS3D.

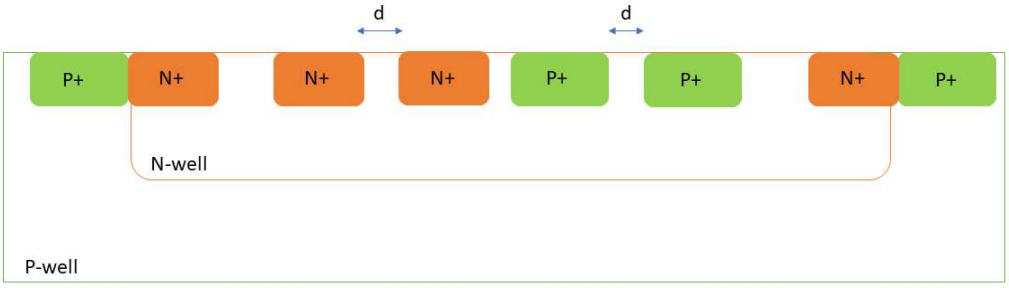

Figure A.2: Diode type 1 (cross section).

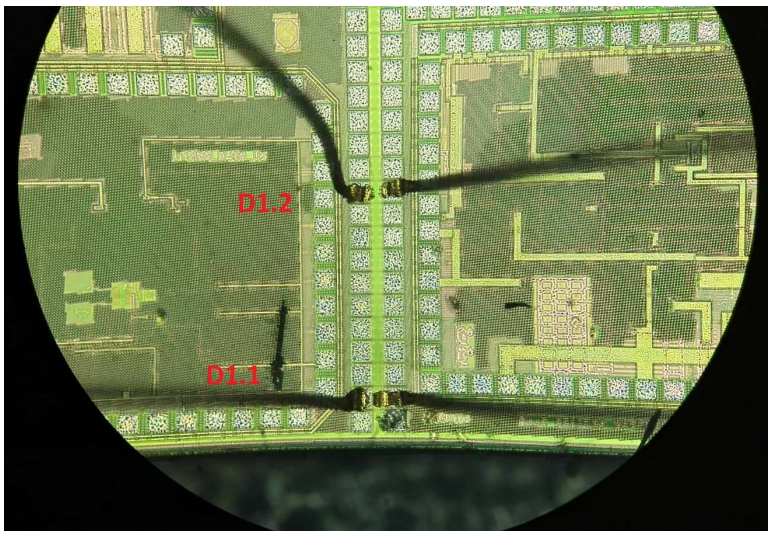

Figure A.3: Diode type 1 seen trough microscope.

Figure A.3 shows that the lower diode, diode 1, has some of the bonding over the active photodiode area. Since this gold comes close to the other bondpad, this gold could expand/shrink during cooling/heating, resulting in a shortcut. Therefore, this diode type 1.1 was not chosen for this research.

Since diode type 1.2 shows close boundaries to the diode on top, diode 1.2 was not chosen for this research.

First measurements

Figures A.4 to A.9 show the photodiode measurement for diode type 1 on the chip (see figure 3.1 in chapter 3).

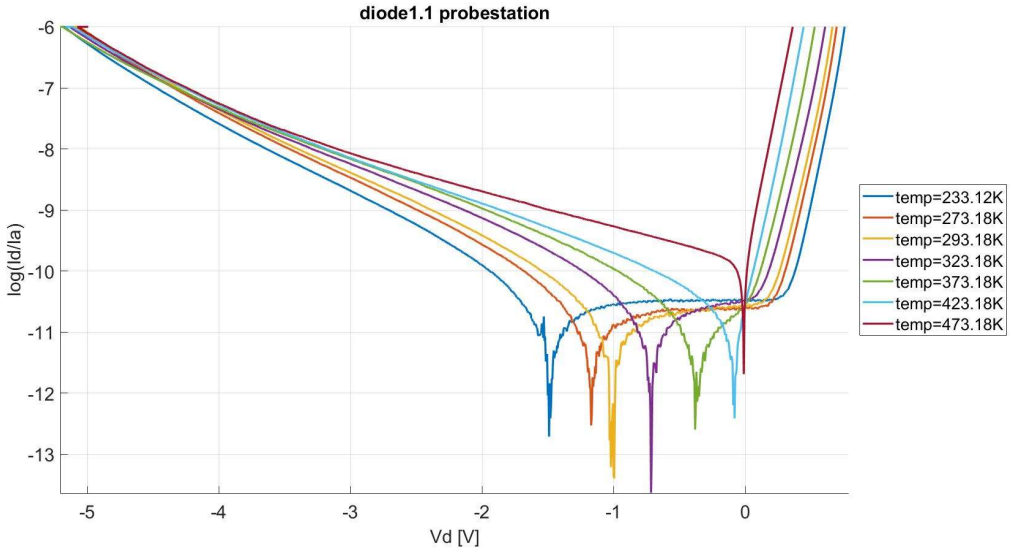

Figure A.4: Diode type 1.1 at dark circumstances for various temperatures.

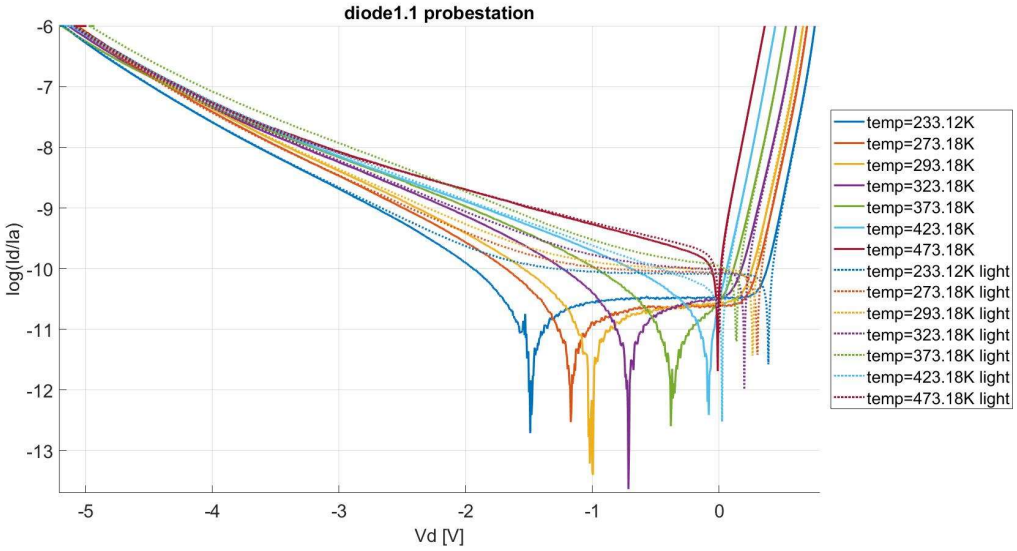

Figure A.5: Diode type 1.1 at light circumstances for various temperatures.

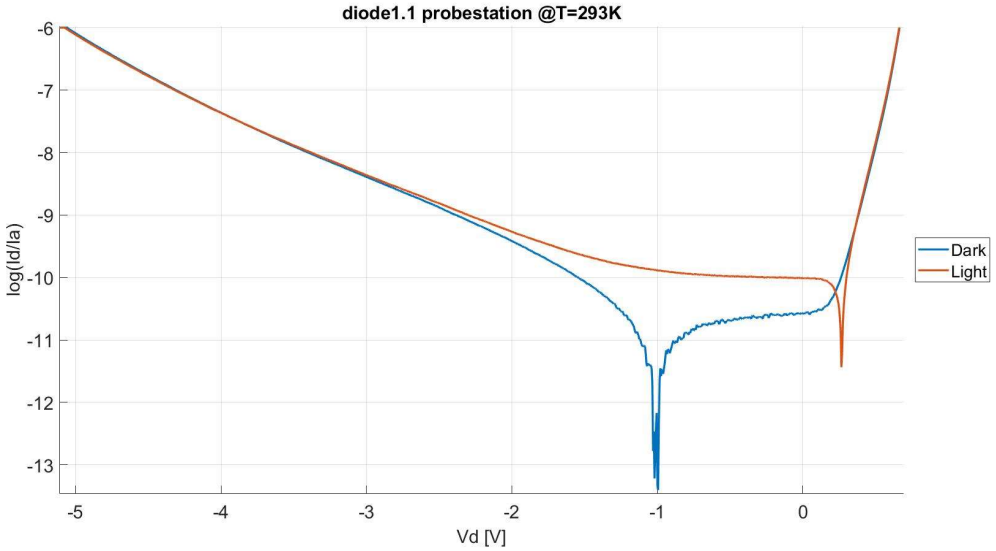

Figure A.6: Diode type 1.1 at dark and light circumstances at T=293.18K.

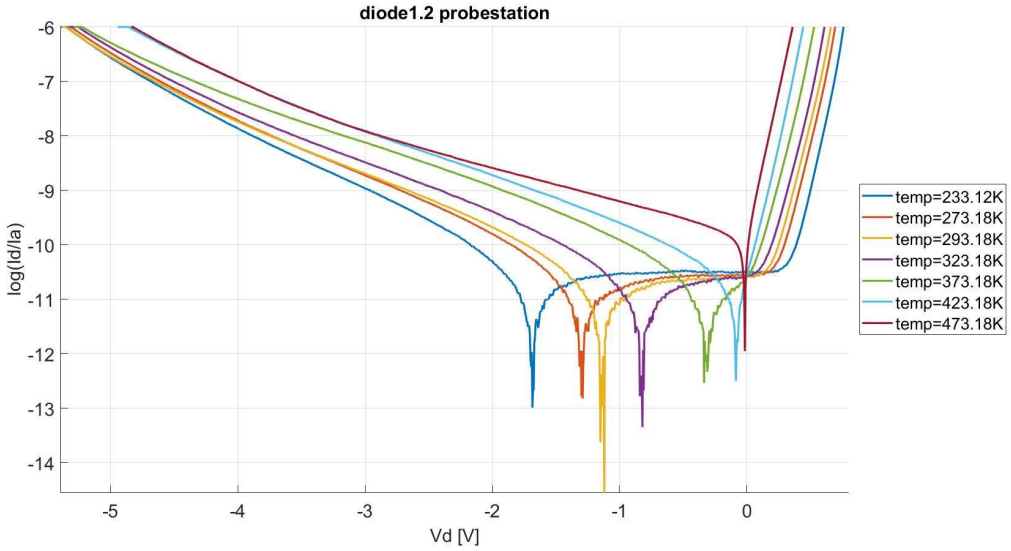

Figure A.7: Diode type 1.2 at dark circumstances for various temperatures.

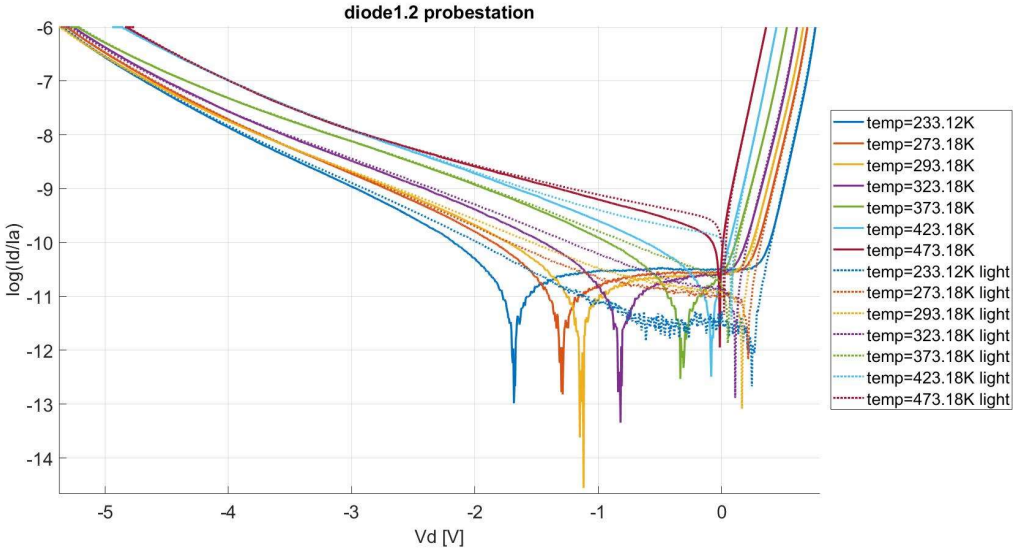

Figure A.8: Diode type 1.2 at light circumstances for various temperatures.

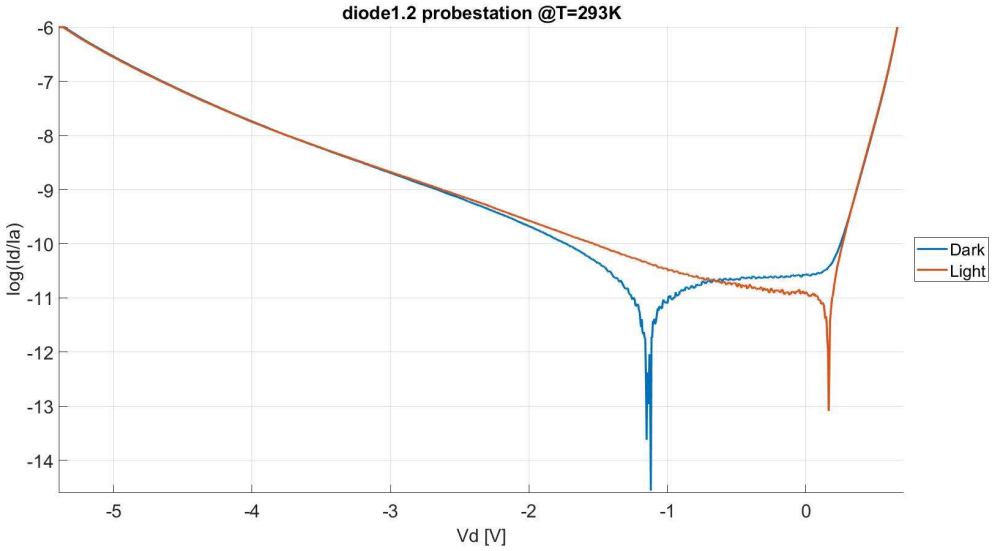

Figure A.9: Diode type 1.2 at dark and light circumstances at T=293.18K.

A.1.2 Diode type 2

Diode type 2 can be found in figure A.10. In this type, the inner p and n region will become larger in width, as can be found in figure A.11 in k. This means that type 1 has the smallest k and type 2 has the biggest k.

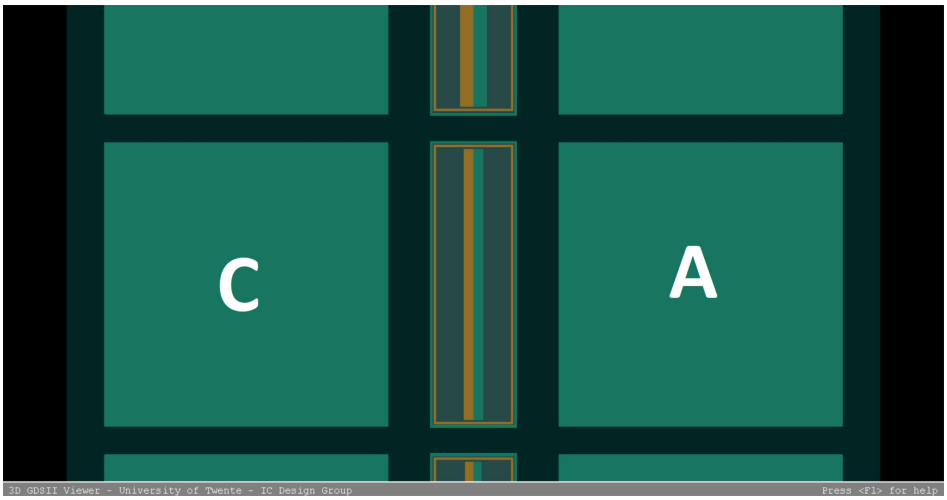

Figure A.10: Diode type 2 (topview) seen from GDS3D.

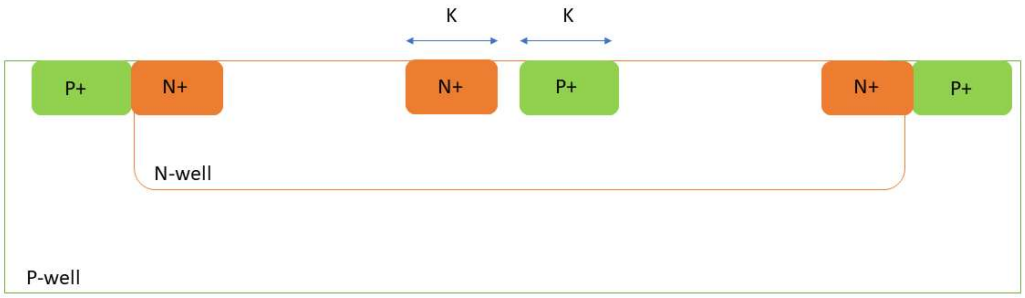

Figure A.11: Diode type 2 (cross section).

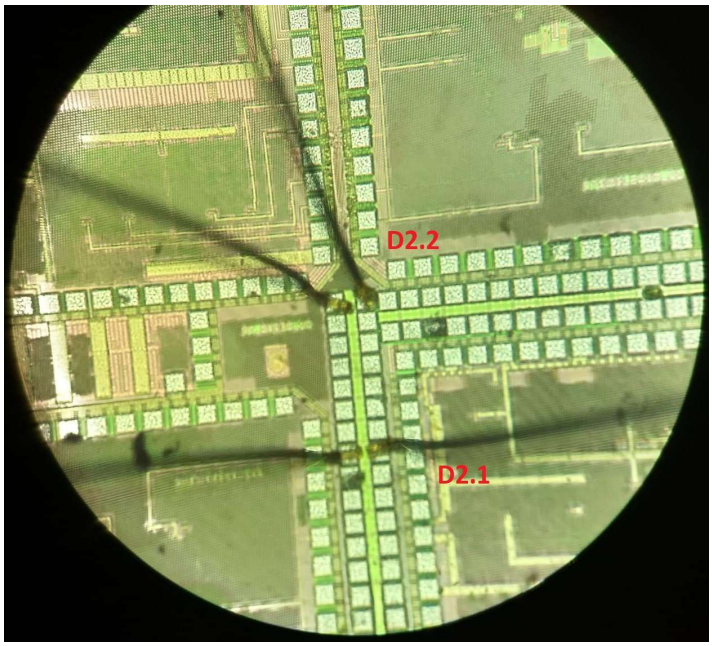

Figure A.12: Diode type 2 seen trough microscope.

Figure A.12 shows that the upper diode, diode 2, has some of the bonding over the active photodiode area. Since this gold comes close to the other bondpad, this gold could expand/shrink during cooling/heating, resulting in a shortcut. Therefore, this diode type 2.2 was not chosen for this research.

Since the structure of diode type 2 is the most common structure and is not gold covered, diode type 2.1 was chosen for this research.

First measurements

Figures A.13 to A.18 show the photodiode measurement for diode type 2 on the chip (see figure 3.1 in chapter 3).

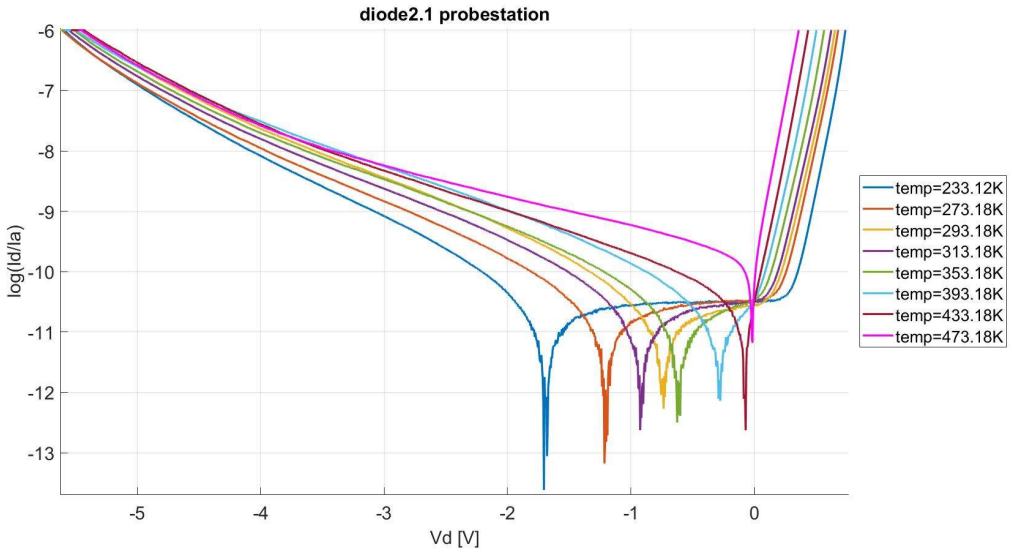

Figure A.13: Diode type 2.1 at dark circumstances for various temperatures.

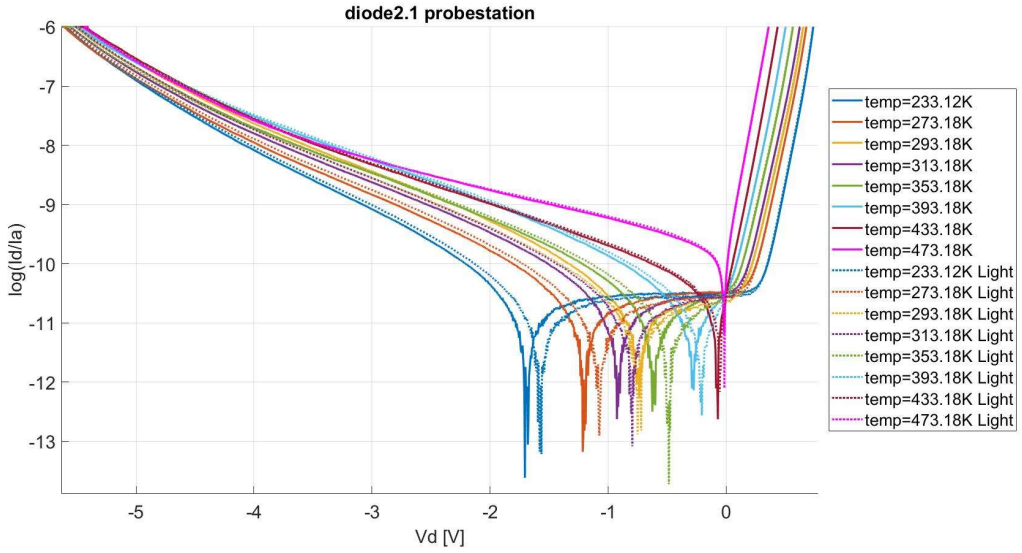

Figure A.14: Diode type 2.1 at light circumstances for various temperatures.

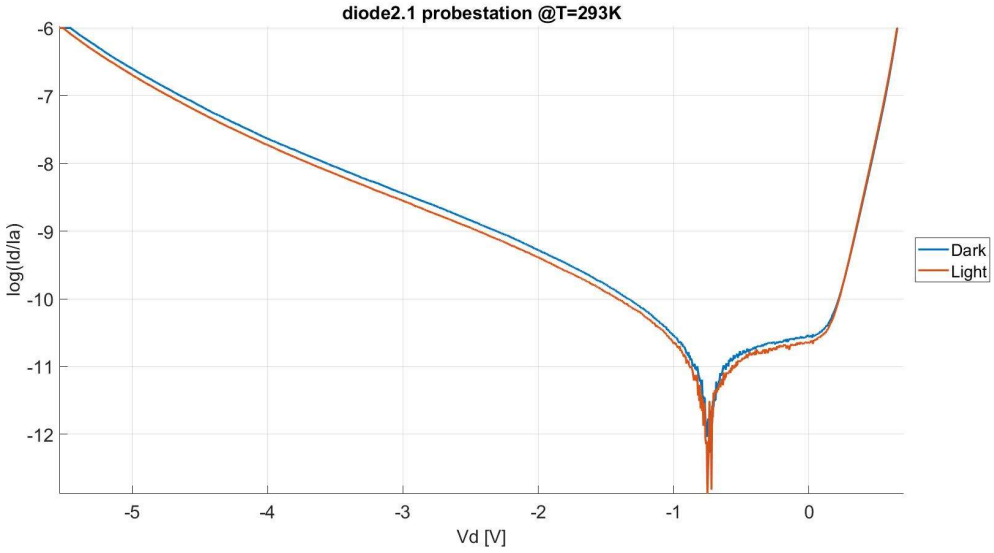

Figure A.15: Diode type 2.1 at dark and light circumstances at T=293.18K.

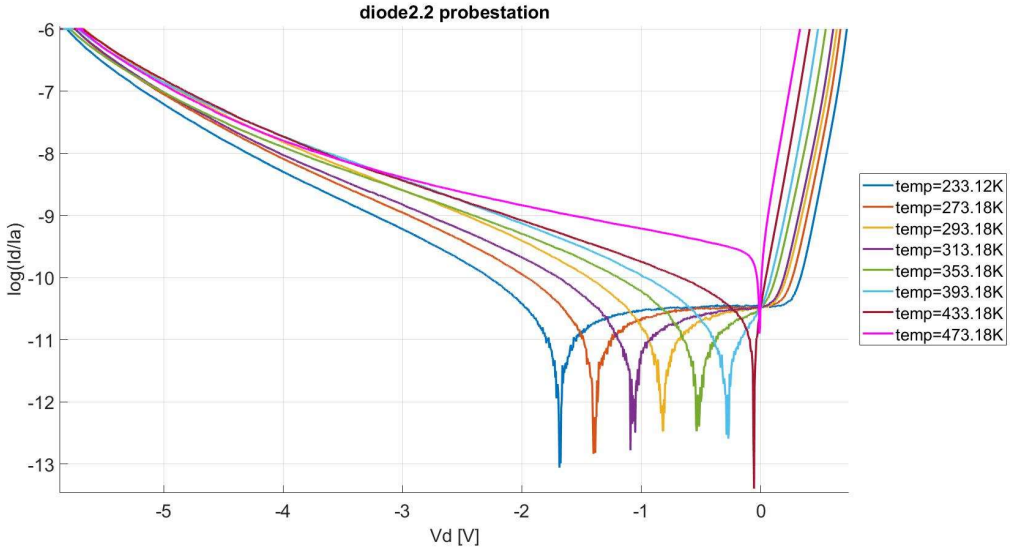

Figure A.16: Diode type 2.2 at dark circumstances for various temperatures.

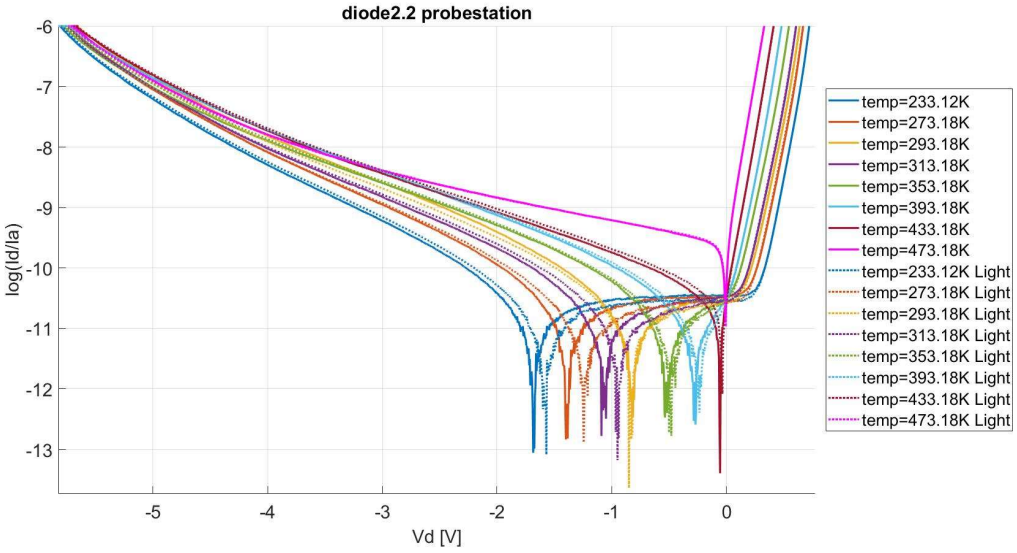

Figure A.17: Diode type 2.2 at light circumstances for various temperatures.

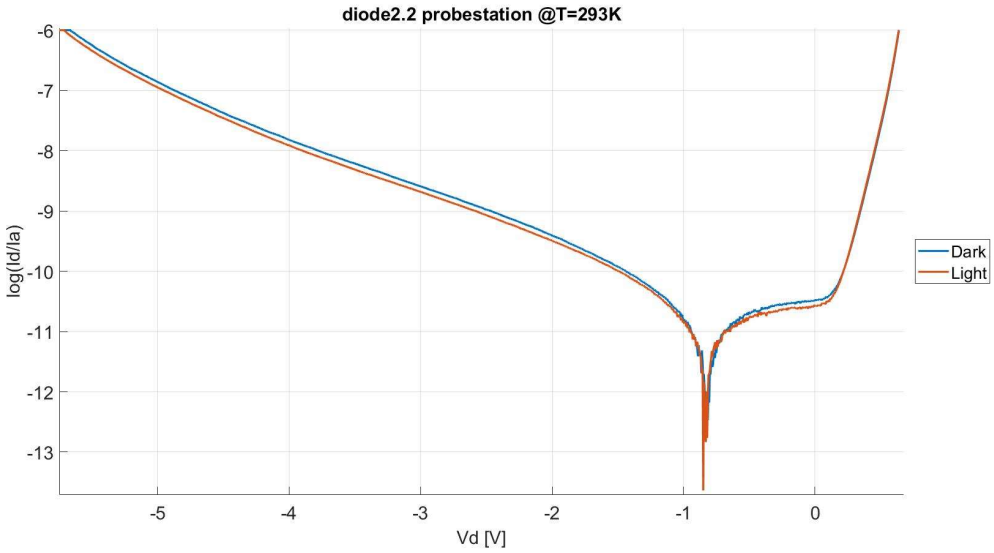

Figure A.18: Diode type 2.2 at dark and light circumstances at T=293.18K.

A.1.3 Diode type 3

Diode type 3 can be found in figure A.19. In this type, the p and n region are located in a square. The size of the square will become larger for different diodes by changing the width of the p region. A cross section of the diode can be found in A.20 This means that type 1 has the smallest p region and smallest square and type 2 has the biggest p region and biggest square.

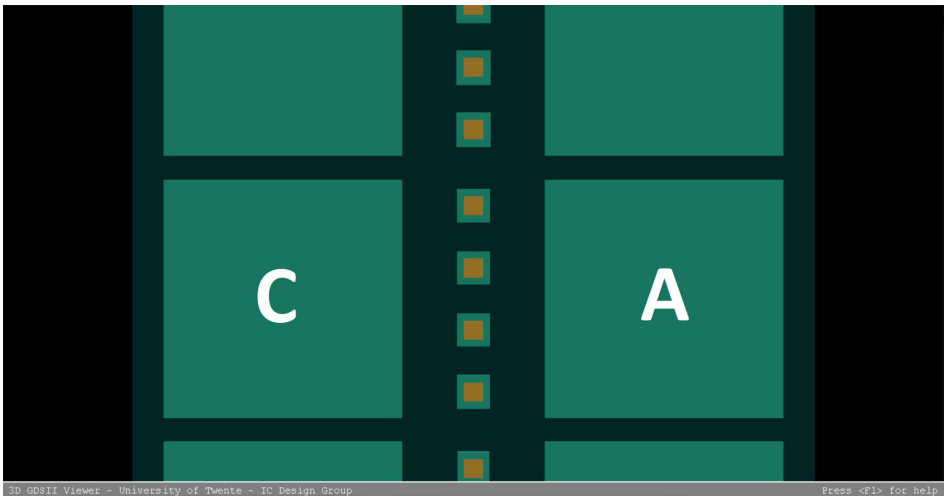

Figure A.19: Diode type 3 (topview) seen from GDS3D.

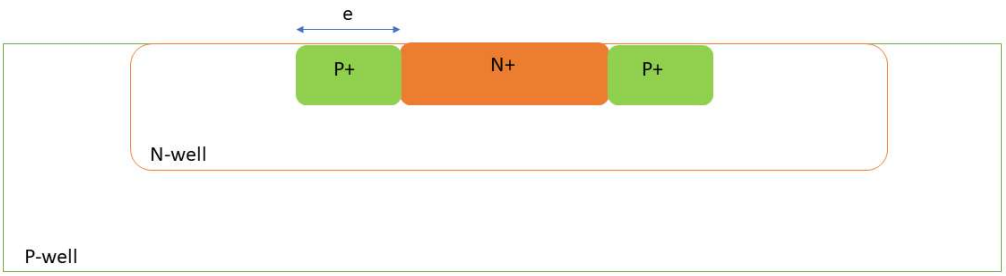

Figure A.20: Diode type 3 (cross section).

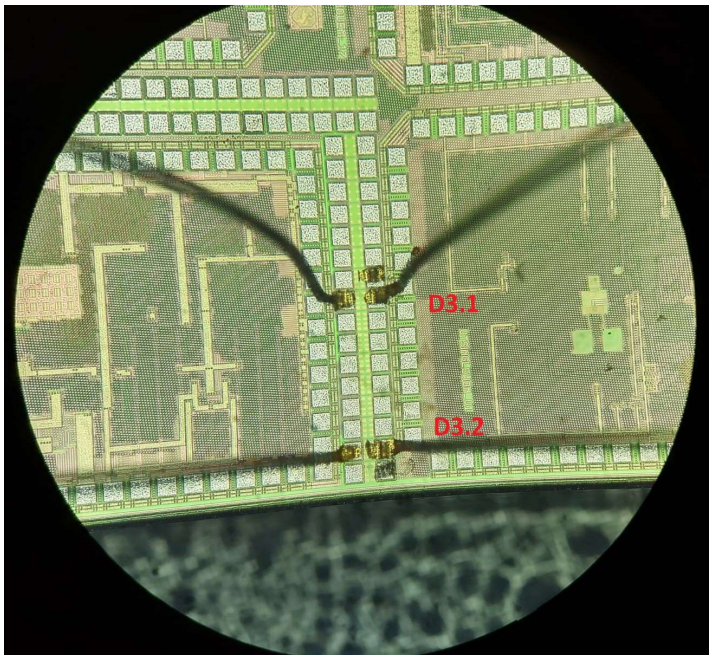

Figure A.21: Diode type 3 seen through microscope.

Figure A.21 shows that the lower diode, diode 2, has some of the bonding over the active photodiode area. Since this gold comes close to the other bondpad, this gold could expand/shrink during cooling/heating, resulting in a shortcut. Therefore, this diode type 3.2 was not chosen for this research. Furthermore, diode type 3.1 shows close boundaries to the diode on top. Expanding or shrinking could lead to measuring two diodes in parallel. This is the reasons why diode type 3.1 was also not chosen for this research. Moreover, the design of diode type 3, the squares, is a design which is scaled in 2 dimensions, which makes research complexer than with scaling in 1 dimension.

First measurements

Figures A.22 to A.27 show the photodiode measurement for diode type 3 on the chip (see figure 3.1 in chapter 3). It is visible that the breakdown voltage increases with increasing temperature. Furthermore, there is some disturbance between the breakdown voltage and the forward voltage. This is most likely noise, but also other circumstances could play a role there.

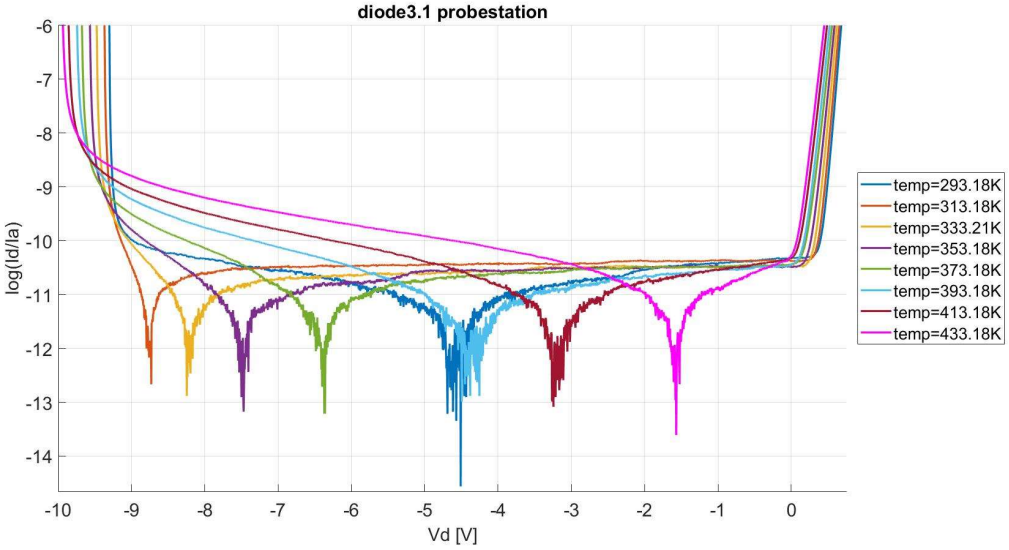

Figure A.22: Diode type 3.1 at dark circumstances for various temperatures.

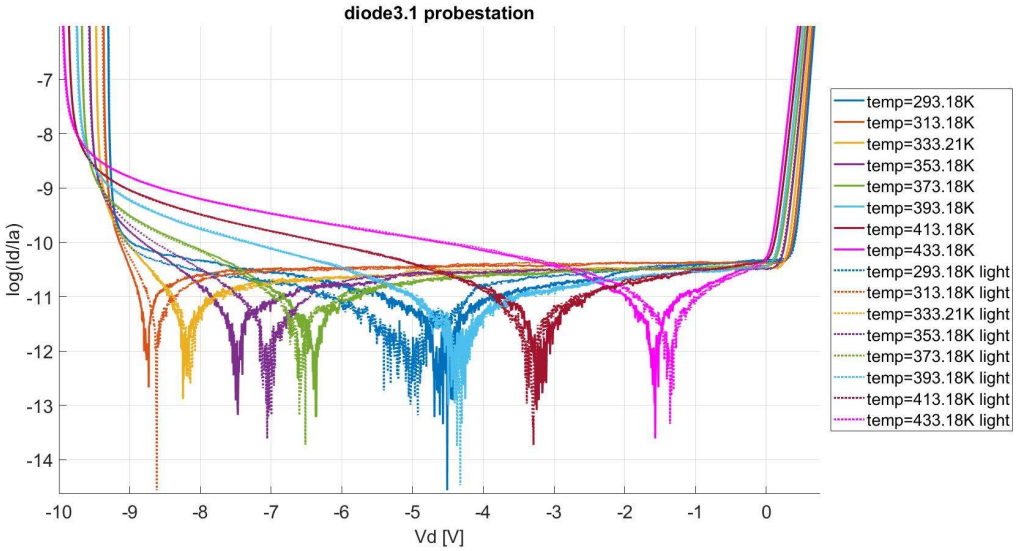

Figure A.23: Diode type 3.1 at light circumstances for various temperatures.

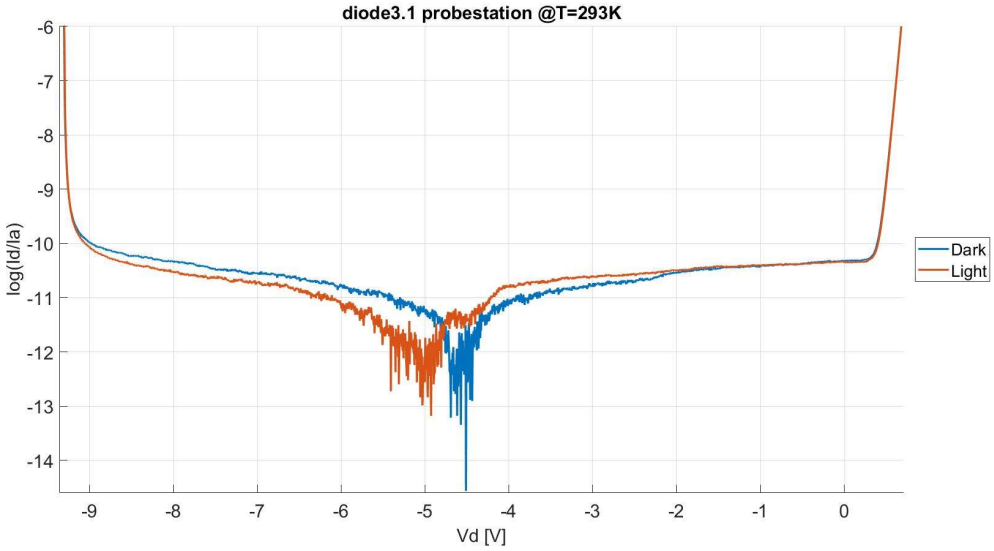

Figure A.24: Diode type 3.1 at dark and light circumstances at T=293.18K.

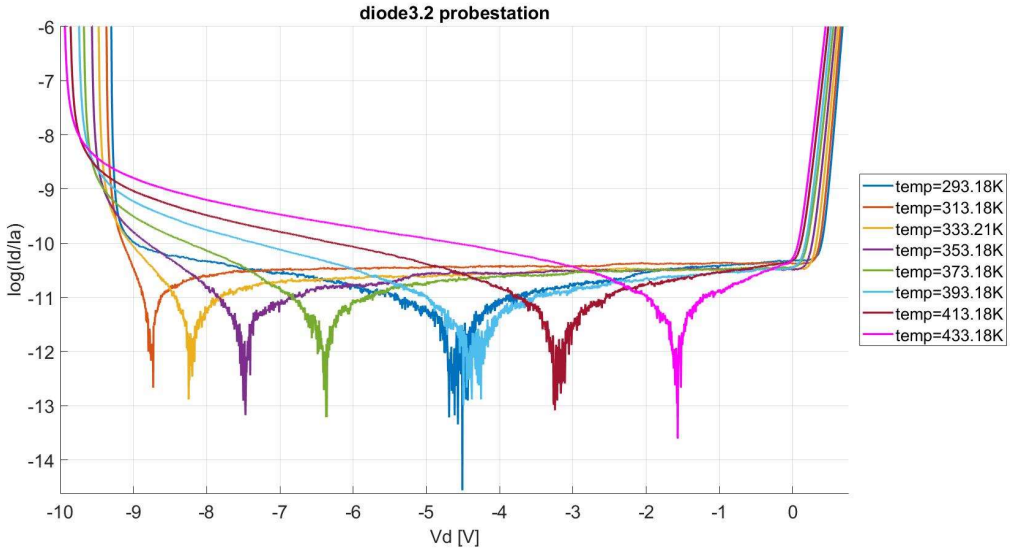

Figure A.25: Diode type 3.2 at dark circumstances for various temperatures.

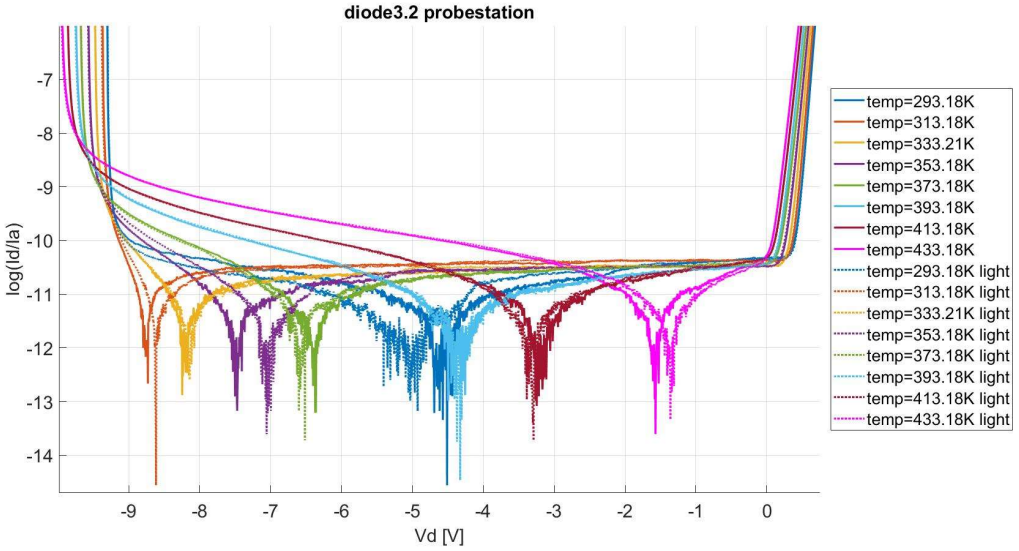

Figure A.26: Diode type 3.2 at light circumstances for various temperatures.

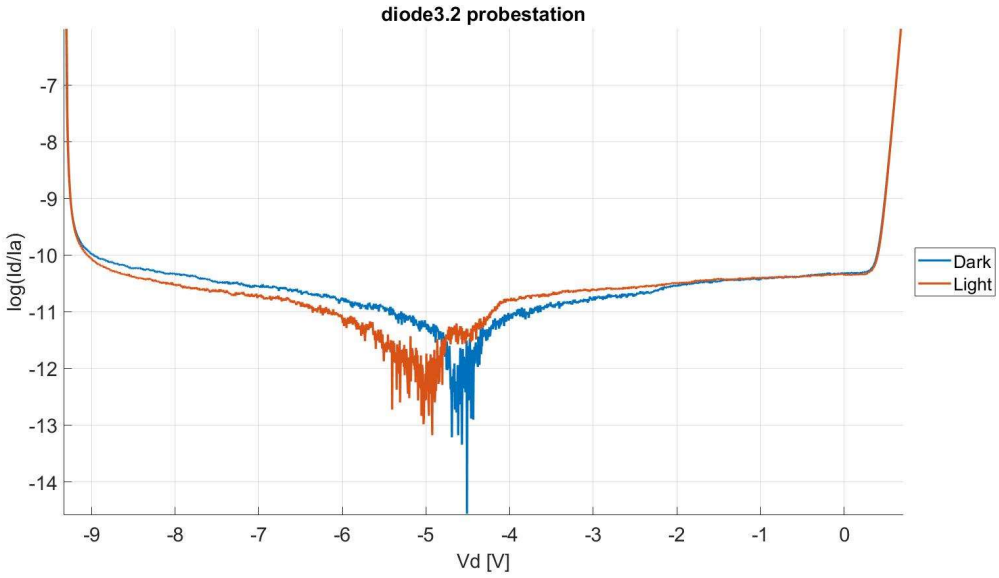

Figure A.27: Diode type 3.2 at dark and light circumstances at T=293.18K.

Appendix B

Measurement equipment

The Keithley 4200 semiconductor characterization system (SCS) has been used for measuring the I-V curves of the photodiode. The SCS needs to be programmed, which can be found in the first part. The second part shows photo's of the measurement equipment used.

B.1 Keithley 4200 semiconductor characterization system

The Keithley 4200 semiconductor characterization system has been programmed the following for all measurements:

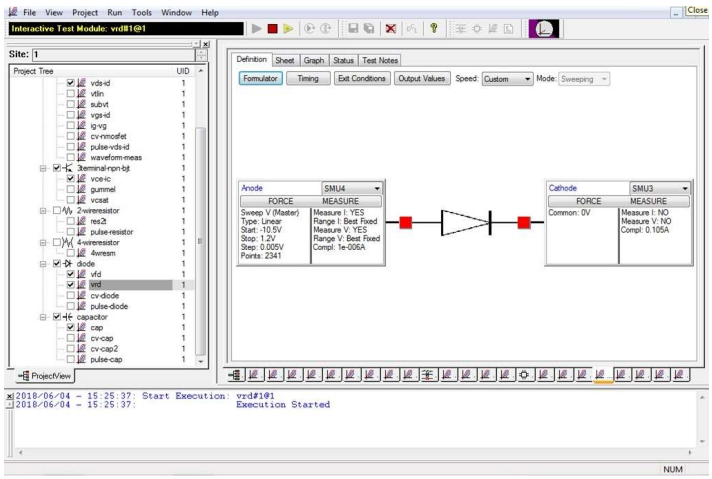

Figure B.1: program for measuring full I-V curve at dark and light circumstances.

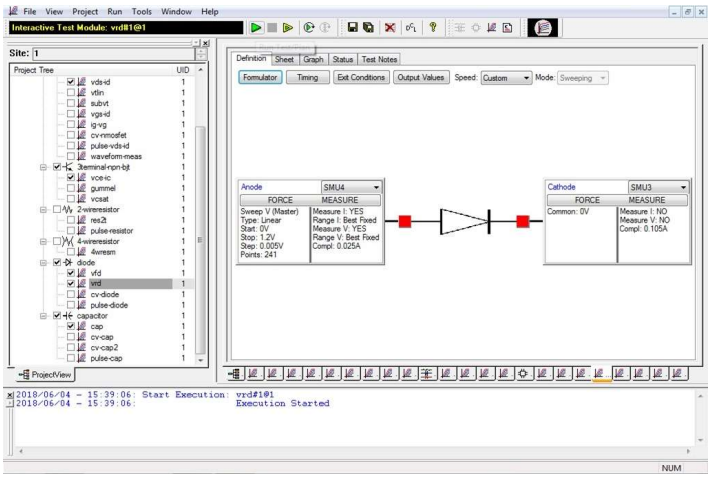

Figure B.2: program for measuring the forward region of the I-V curve at dark circumstances.

As is visible in figure B.1, the compliance has been set to 1 μA in order to avoid damage to the photodiode at avalanche. In the forward measurement, this compliance is changed to 0.025 A as is visible in figure B.2. The speed of the measurements has been customized. The delay factor is 1.3, the filter factor is 2 and the A/D aperture time is 1 PLCs.

B.2 Photo's measurement devices

Figure B.3: measuring the electrical characteristics. Probe station opened.

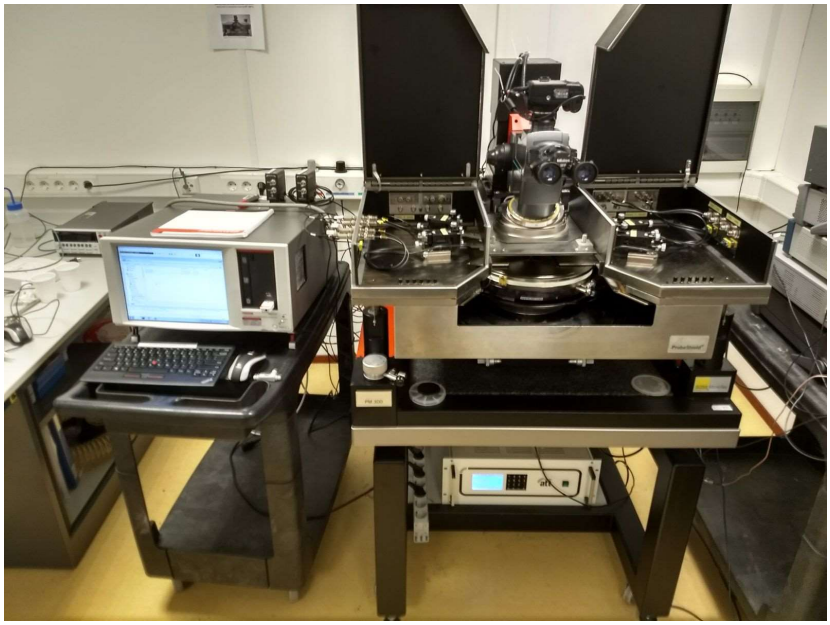

Figure B.4: measuring the electrical characteristics. Probe station open with Keithley 4200-SCS.

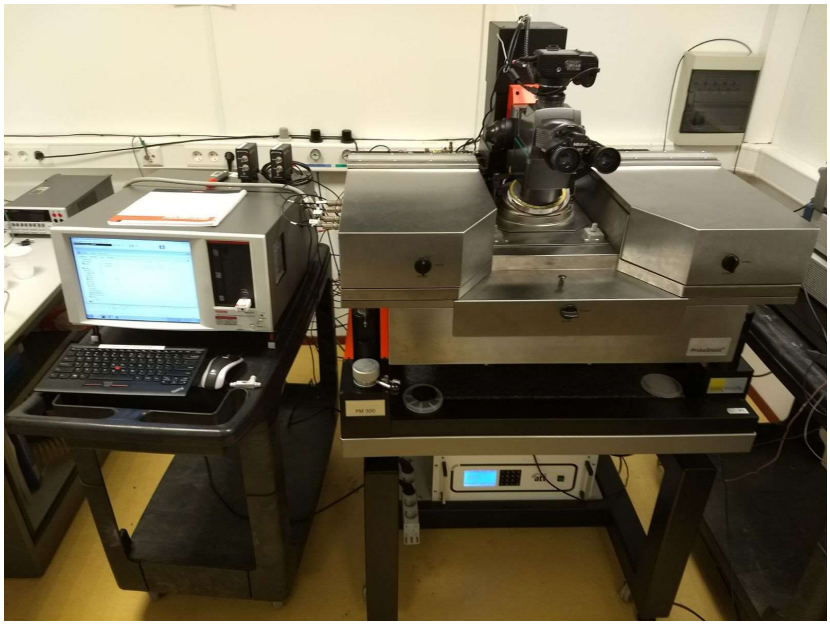

Figure B.5: measuring the electrical characteristics.Probe station closed with Keithley 4200-SCS.

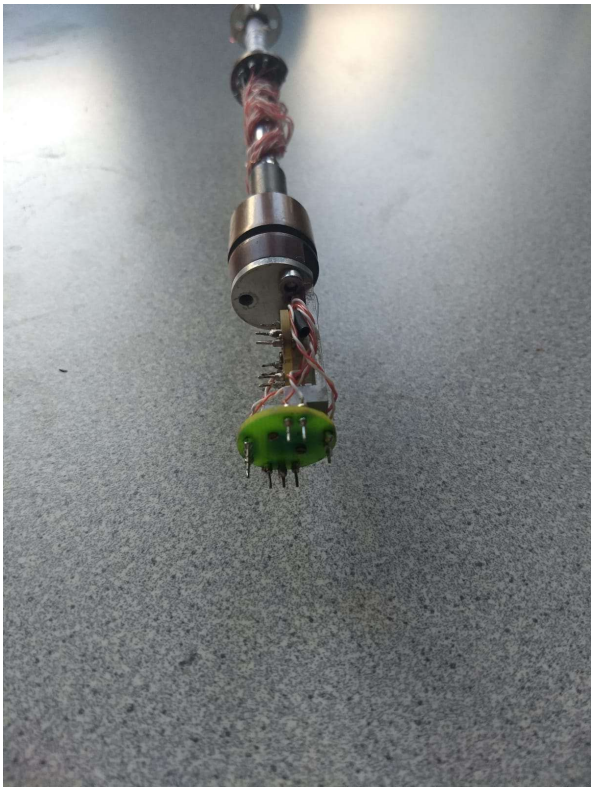

Figure B.6: sample holder on the cryostat.

Figure B.7: full inside holder of the cryostat.

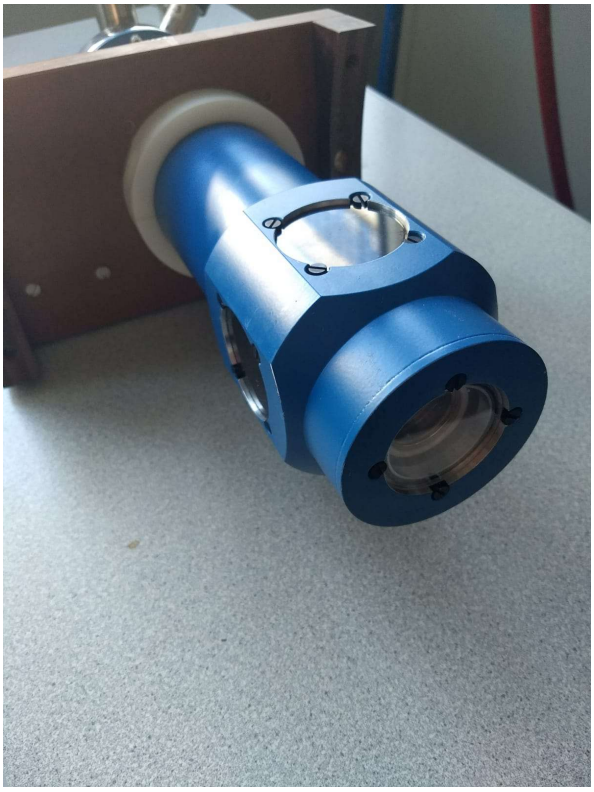

Figure B.8: cryostat with five windows.

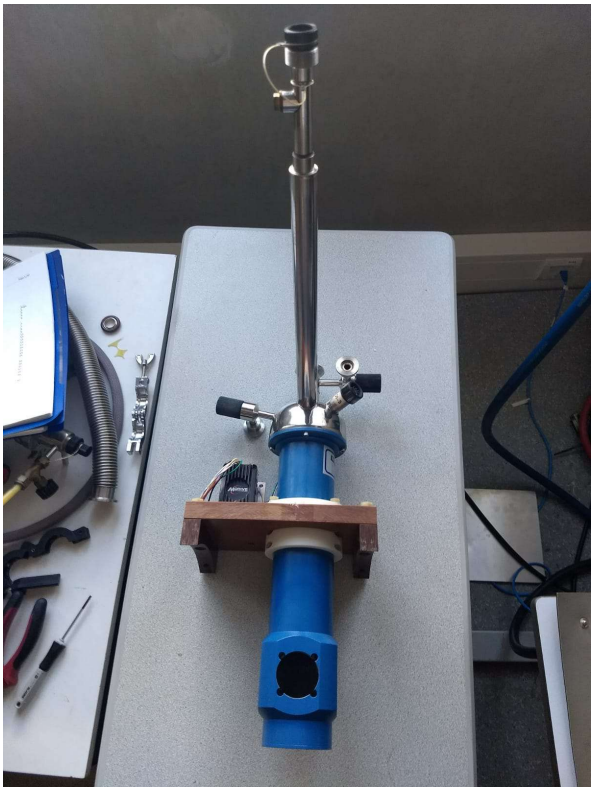

Figure B.9: cryostat with five windows.

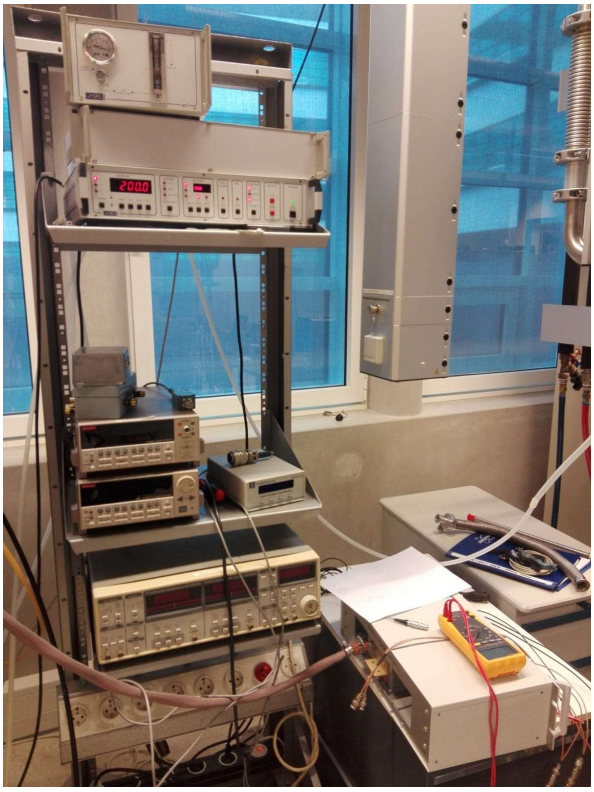

Figure B.10: cryostat temperature and flow control.

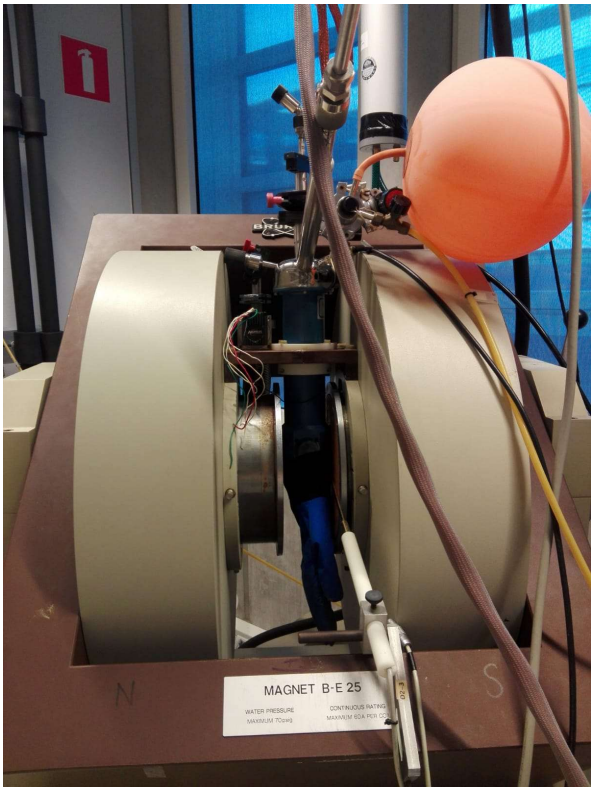

Figure B.11: cryostat in holder and connected.

Appendix C

Optical measurements

Since the monochromator could not be used given the time span, a self made optical set-up was built.

C.1 Theoretical set-up

Figure C.1 shows a diagram of the optical set-up. The set- up has as the light source, with a fiber optical cable in order to aim the light. This light is aimed at the first lens, such that the light focuses on the slit. Before the slit, a longpass coloured glass filter is positioned. This filter blocks out second and third orders of certain frequencies (later on more about this). The light from the slit then goes to the second lens which collimates the bundle of light. This bundle will go the reflective grating. The reflection grating splits and reflects the light in several beams. Each of these beams contain a specific wavelength of a wide spectrum. By separating the wavelengths with the third lens, specific wavelengths can be focused on the second slit. Via a fourth lens, the light reaches the mirror to beam the light upwards to the cryostat. Here the light will see the fifth lens, which focuses the light on the cryostat.

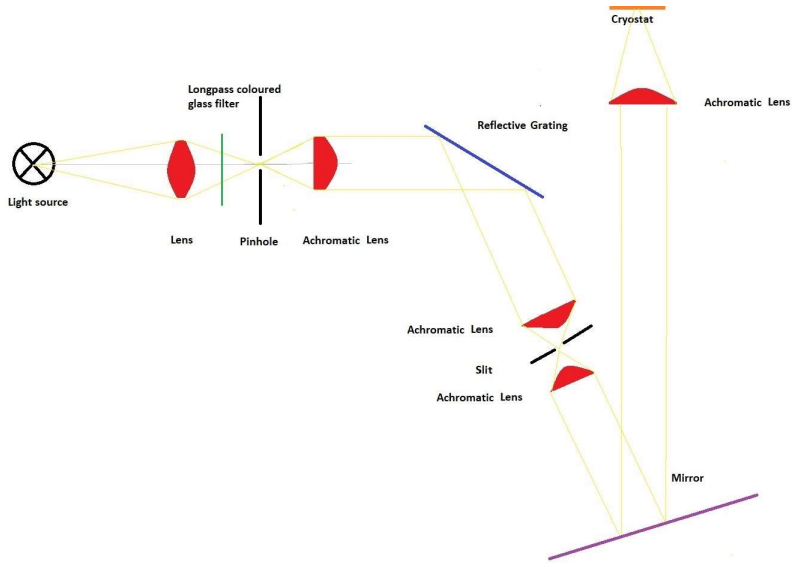

Figure C.1: schematic of the optical measurement set-up.

C.2 Calculations

For this set-up, several calculations need to be done and choices need to be made. These calculations and decisions will involve the reflective grating angles, the slit width and the focal length.

First the reflective grating. The reflective grating makes use of equation C.1. Knowing this equation, this can easily be plotted. The values for total angle between the incident angle and the exit bundle of the order of interest and the grating density can be chosen depending on own preference. For this set-up, a grating density of 600 lines/mm and a total angle of 105°is chosen. This results in the plot shown in figure C.2. From this graph, it can be seen at which angle the reflective grating needs to be placed according to the wavelength wanted. Since this research will focus on the wavelengths between 400 and 1200 nm, the angle between the incident light bundle and the normal of the grating will change between 15 °and 41 °. However, as is visible in figure C.2, the second and third order of other wavelengths influence the first order wavelengths as well. Therefore, a longpass coloured glass filter is needed. In this case, the FGL645 will be used for the wavelengths 700 to 1200 nm and the FGL400 for the wavelengths 400 to 700 nm. The FGL645 will block all wavelengths lower than 700 nm, meaning that the second order influence of 1200 nm will be blocked. The same principle is true for the FGL400.

$$\lambda \mathrm{m} = a \cdot (sin(\Theta_\mathrm{i}) - sin(\Theta_\mathrm{m})) \tag{C.1}$$

$$\Theta_m = \Theta_\mathrm{t} - \Theta_\mathrm{i}$$

With: exit angle with respect to the grating normal [°] (Θ_m), angle of the normal of the grating with respect to the incident angle of exit [°] (Θ_i), total angle between incident angle and the exit bundle of the order of interest (Θ_t), grating period derived from the grating density (a), and order of the wavelength of interest (m)

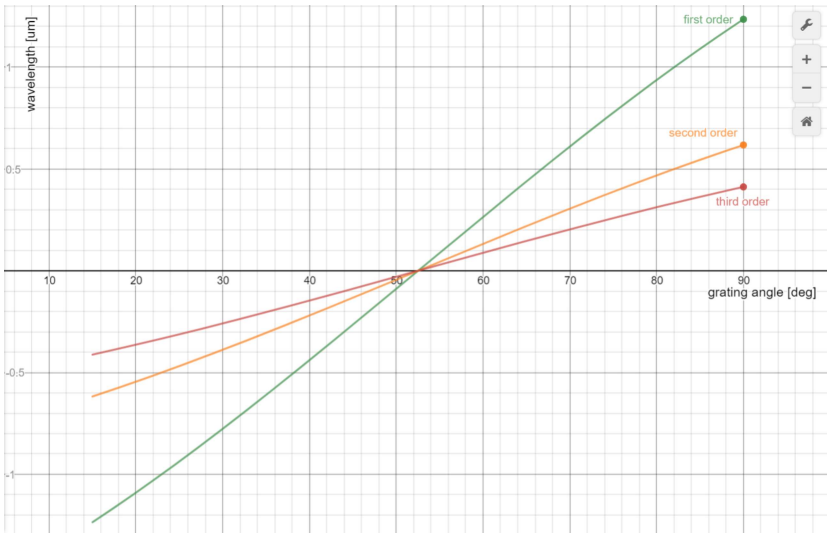

Figure C.2: plot for the different reflective grating angles according to the different wavelengths. Showing the first, second and third order of the wavelengths.

From figure C.2, the bundle diameter can also be found. The slope of the first order plot is approximately 33 nm per degree. This means that the wanted angle resolution is 0.03 degrees or 0.5 mrad.

This means that the minimum bundle that will hit the grating, should be 5 mm (seeing equation C.2). When having a lens of 25 mm height, this will not be a problem.

$$\text{angular resolution} = 1.22 \cdot \frac{\lambda}{D_{\text{bundle}}} \tag{C.2}$$

Where diameter of the light bundle [mm] (Db)

Moreover, the lens' focal point needs to be determined. Depending on the distance available, the focal point of the lens can be chosen. Since the set-up should not become too large, a focal length of 100 mm has been chosen.

Furthermore, the slit width needs to be determined. The bandwidth that will reach the cryostat will depend on the slit width. The smaller the width, the smaller the bandwidth of the light bundle. However, the intensity of light will also lessen by decreasing the slit width. A compromise between light intensity and light bandwidth needs to be made [22]. Equation C.3 shows the steps to find the size of the slit. Since the lenses will all be chosen the same, there is no need to have different slits/pinholes. Therefore, the slit and pinhole will have a size of 50 μm

$$\begin{aligned} \text{angular resolution} &= 1.22 \cdot \frac{\lambda}{D} \\ 0.5\, m\, rad &= \frac{\text{slit width}}{100\, mm} \\ \text{slit width} &= 50\, \mu m \end{aligned} \tag{C.3}$$

Where distance between slit and lens [mm] (D).

Finally the position of the mirror needs to be chosen. Since the lenses, splits and grating will be aligned on the horizontal plane, the mirror needs to be positioned with a 45 °angle upwards. Moreover, the angle according to the grating needs to be determined. Since calculating this cost some time, the mirror will be positioned during the building process such that the light is focused to the lens of the cryostat, keeping in mind that the total angle of the reflective grating is 105 °.

C.3 Actual set-up

A photograph of the actual set-up can be found in figure C.3. The set-up has some changes. The total angle is 45 °instead of 105 °, due to advantages making the dark box around the 'monochromator'. This is possible since the angle was free to chose.

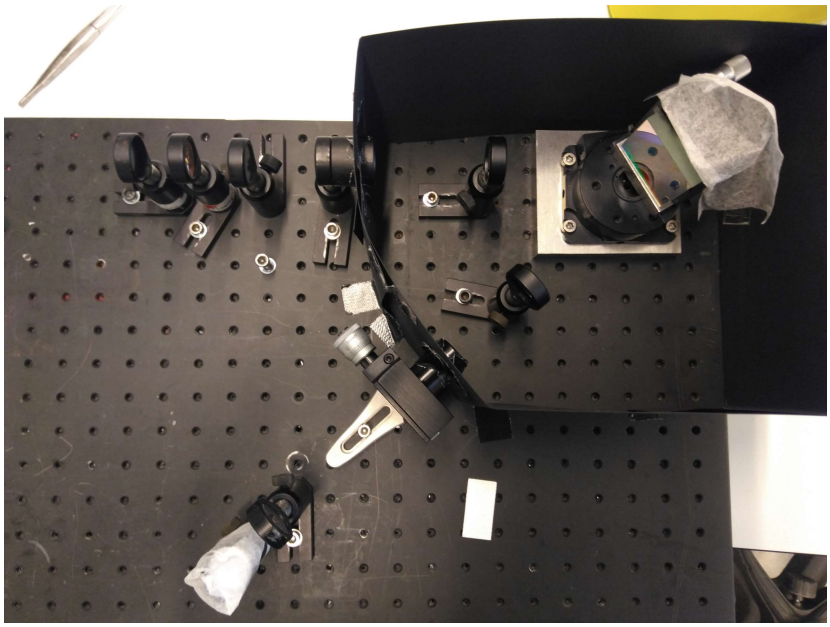

Figure C.3: topview of the real optical set-up.

Unfortunately, the intensity of light coming out of the slit appears to be too low for reaching the next lens. The outcome of the slit, close to the slit, can be found in figure C.4. This could have been improved by choosing bigger pinholes and slits. However, that would result in a broader bandwidth.

Figure C.4: rainbow outcome of the monochromator.

In order to still have illumination measurements, a fiber light source (intralux 6000-1) has been used with full intensity, close to the window of the cryostat. In this way, dark and light circumstance measurements could be preformed.